



**Politecnico  
di Torino**

**Politecnico di Torino**

Master's degree in Biomedical Engineering

A.Y. 2024/2025

Graduation session March 2025

# **Design of a vascularized *in vitro* skin model to mimic metastatic melanoma**

Supervisors:

Prof. Mattu Clara

Prof. Ciardelli Gianluca

Dott. Mattioda Carlotta

Candidate:

Brunialti Luca



## Abstract

Melanoma is a skin cancer that arises from genetically altered or activated epidermal melanocytes. The prognosis of patients who reach the metastatic phase (stage IV) is grim, presenting a 5-years survival rate between 5% and 19%, depending on the site and extent of the metastatic disease.

Currently, there is no definitive cure for metastatic melanoma, and existing treatments are hindered by drug resistance and significant side effects. Moreover, advanced treatment options often fail because of transport limitations, poor targeting capacity, and side effects. The traditional drug testing models mainly based on oversimplified 2D or 3D cell cultures failed in supporting the drug development process, because of their lack of similarity with the complex pathophysiology of the metastatic disease.

This work aims at developing an *in vitro* three-dimensional dynamic model of metastatic melanoma through microfluidic technology. A custom-made microfluidic chip composed by three chambers connected in series was designed. A primary melanoma model was cultured in the first chamber which is linked to the other chambers through a microfluidic channel. The two additional chambers can host matrices mimicking frequent targets of melanoma metastases, such as brain, lung or bone. To obtain the primary melanoma model, first a dermis mimic was prepared using a collagen/hyaluronic acid-based hydrogel seeded with human dermal fibroblasts (Hff-1), covered with a layer of keratinocytes (HaCaT), to reproduce the epidermis.

In details, the obtained hydrogel was composed of type I bovine collagen and methacrylate hyaluronic acid (HAMA), able to successfully mimic the mechanical and biological properties of the dermis. The hydrogel successfully reflected the native extracellular matrix proprieties, as confirmed by rheological characterization and viability test. The model, cultured for up to 21 days, was able to host different cell populations, as confirmed by immunofluorescence analysis.

An endothelial cells layer was cultured in the basal surface of the hydrogel to mimic the endothelial layer of blood vessels and to induce the development of vessel sprouts within the dermal compartment. A spheroid of melanoma cells (SK-MEL) was incorporated in the dermal compartment to mimic the initial stage of the pathology.

To achieve a mature endothelial layer the model was exposed to dynamic flow provided by a pump, supplying an essential stimulus for the development of the vasculature. Confocal microscopy analysis confirmed the presence of a dense and aligned endothelial layer, as well as the development of a capillary network within the hydrogel.

The obtained 3D melanoma model represents a physiologically relevant environment for studying tumour progression in a more ethical and cost-effective way.

Future developments include the optimization of the metastatic compartment and the employment of the model as a validation platform for innovative drug-delivery systems.

## Table of figures

Figure 1: structural anatomy of skin showing the three main layer: epidermis, dermis and the subcutaneous tissue. Illustration created with BioRender.com.....	13
Figure 2: Schematic representation of the progression stages of melanoma. Stage I present a localized melanoma. In Stage II there is cancer growth and cellular expansion. Stage III led to cellular spreading in the nearby tissues with the involvement of lymph nodes. Metastatic cells begin their spreading through the organism in stage IV. Illustration created with BioRender.com. ....	15
Figure 3: Schematic representation of melanoma genesis. Exposure to UV radiation triggers keratinocytes to send activation signals to melanocytes, stimulating melanin production. This pigment plays a crucial role in protecting melanocytes from UV-induced DNA damage. However, in some cases, this protective mechanism is insufficient, leading to DNA mutations in melanocytes. In the most severe cases, these mutations result in the transformation of melanocytes into melanoma cells. In other instances, mutated melanocytes develop into benign nevi cells, which, over time, may still acquire further mutations and progress into melanoma.[12] .....	16
Figure 4: Schematic diagram of the tumour microenvironment. The tumour microenvironment is a complex ecosystem composed of heterogeneous components, including tumour cells, stromal cells, various types of immune cells, soluble molecules, and extracellular matrix (ECM) components.[53] .....	17
Figure 5: Illustration of melanoma spheroids treated with different concentration of Nebivolol. As the drug concentration increases tumour cells presents a higher apoptotic behaviour. Cell viability seems to decrease already at 25 $\mu\text{M}$ . [38] .....	21
Figure 6: Schematic representation of the HSE. The bottom layer presents the dermal compartment composed by fibroblast seeded hydrogel. On top of that there is the epidermis model composed of keratinocytes seeded on top of the dermal model, maturated on correspondence of air-liquid interface.[41].....	22
Figure 7: Proliferation, migration and invasiveness of melanocytes in an HSE at 0, 9, 15, 20 days. Black arrows and inset images highlight positive staining. The scale bar in the main images shows 100 $\mu\text{m}$ , and the width of the insets are approximately 75 $\mu\text{m}$ . [42].....	23
Figure 8: Exploded view of a melanoma on chip device and its flow diagram scheme, representing the volume injection procedure.[46] .....	25

Figure 9: Schematic representation of the primary tumour model assembly. a) seeding of Hff-1 cells inside the Col-HAMA gel to produce the dermal model. b) Positioning of the dermal model inside a transwell. c) Installing of the melanoma spheroid inside the dermal model for the creation of the tumour model. d) Seeding of keratinocytes on top of the dermal layer to mimic the epidermal model. e) Seeding of endothelial cells on the bottom side of the transwell membrane to mimic the vascular system. f) Introduction of the system in the microfluidic chip to assure the dynamic condition. Illustration created with BioRender.com .....26

Figure 10: Schematic illustration of the reticulation process of both Col-HAMA (80:20) and Col-ColMA-HAMA (40:40:20) formulations. Illustration created with BioRender.com.....29

Figure 11: Schematic representation of the protocol for the derivation of the wet degradation data of the Col-HAMA (80:20) hydrogel. Illustration created with BioRender.com .....32

Figure 12: Schematic representation of the step toward the creation of the epidermal model. After the 7 days maturation of the dermal model, a layer of keratinocytes was placed on top of the Col-HAMA hydrogel and incubated for 4 days in medium. Then the medium on top of the layer was removed to create the air-liquid interface typical of in vivo skin. Illustration created with BioRender.com .....34

Figure 13: Schematic representation of the procedure to obtain the melanoma model. The key procedure is the integration of a SK-MEL spheroid within the dermal model. Illustration created with BioRender.com .....35

Figure 14: Illustration of the indirect co-culture protocol. Hff-1 and SK-MEL cells were seeded simultaneously in separate flasks. Once they reached confluence, they were transferred to a well of a 24-well plate and a Transwell insert, respectively. After 1 day of culture, the Transwell insert was placed into the multiwell, and the system was incubated for an additional day. Illustration created with BioRender.com .....36

Figure 15: Illustration of the melanoma conditioned medium protocol. Conditioned medium is withdrawn from a melanocytes-seeded flask. Hff-1 were incubated under normal RPMI (CTRL) and conditioned RPMI. Illustration created with BioRender.com .....37

Figure 16: Method for endothelial layer characterization on the bottom side of a transwell membrane. Two conditions were investigated, the static and the dynamic. The static condition was explored by placing the transwell in a 24-multiwell, whereas the dynamic condition was explored by using the microfluidic chip. Illustration created with BioRender.com .....38

Figure 17: Protocol for generating a vascularized dermal model. After the seeding of the Col-HAMA formulation with fibroblast and after its 7 days maturation, endothelial cells were seeded on the bottom side membrane of the transwell, with 4-hour static incubation to permit cell adhesion. After that the system was placed inside the microfluidic chip and incubated for different time points. Illustration created with BioRender.com .....39

Figure 18: Schematic representation for the administration procedure of NPs. Illustration created with BioRender.com .....40

Figure 19: Hydrogel's storage modulus behaviour during frequency sweep test. After an initial phase of photo reticulation of 60 seconds the three formulations undergo a 30-minute phase of thermoreticulation.....41

Figure 20: Graphic of the Strain sweep tests conducted on a) Col-HAMA (80:20) and b) Col-ColIMA-HAMA (40:40:20). The tests were performed over a strain range from 0.01% to 1000%. For both formulations the LVE region ends at 1% of strain. The  $\gamma_f$  begins at around 1000% and 700% respectively for Col-HAMA and Col-ColIMA-HAMA.....42

Figure 21: Graphic representation of relative cell viability obtained through CellTiter Blue assay. The Col-ColIMA-HA samples present the worst viability results whereas the Col-HAMA formulation presents good biocompatibility properties. ....44

Figure 22: a) Wet weight variation % of Col-HAMA (80:20) formulation. The graphic shows an initial increase of the gel weight, this is mainly due to the swelling process that the gel undergoes in the initial hours. The y-axis represents the weight variation percentage, ranging from 50% to 150%. b) Dry weight variation % of Col-HAMA (80:20) formulation. The gel initially undergoes a rapid decrease in dry weight, likely due to hydrolytic degradation that begins immediately upon exposure to the surrounding environment. After this initial phase, the gel stabilizes and eventually reaches a plateau, indicating a slower degradation rate or equilibrium in the process. The y-axis represents the weight variation percentage, ranging from 0% to 100%. ....45

Figure 23: Immunofluorescence analysis of human collagen and fibronectin deposition. The control does not exhibit any human collagen presence. Whereas, starting from day 7, fibroblasts deposit their own matrix as collagen and fibronectin are markedly expressed.....46

Figure 24: Immunofluorescence analysis of the epidermal layer. Top view. Keratinocytes have proliferated until the creation of a uniform layer. ....47

Figure 25: Immunofluorescent illustration of the epidermal layer model on top of the dermal model. ....48

Figure 26: Confront between a) SK-MEL in Hff-1 seeded COL-HAMA hydrogel and b) SK-MEL in COL-HAMA hydrogel. In both condition the SK-MEL spheroid shows an inclination to expand and invade the surroundings environment. The main difference lies in the .....	49
Figure 27: Fluorescence images of Hff-1 and SK-MEL after a 7-day co-culture at different zoom. a) 10x enlargement. b) 20x enlargement.....	50
Figure 28: Comparison of collagen and fibronectin expression between SK-MEL only SK-MEL+Hff-1 samples. a) SK-MEL spheroid in Col-HAMA hydrogel at 20x and 60x enlargement. In this case there is no collagen and fibronectin expression as the Hff-1 responsible for their deposition are absent. b) SK-MEL spheroid in Hff-1 seeded COL-HAMA hydrogel at 20x and 60x enlargement. The fibroblast engulfed inside the tumour spheroid have deposited collagen and fibronectin.....	51
Figure 29: immunofluorescence analysis of CAF cells in different conditions. a) The control does not show any fluorescence to $\alpha$ -SMA. b) Conditioned medium culture. The fibroblasts were cultured with melanocytes conditioned medium. The filaments of $\alpha$ -SMA are visibly expressed. c) Indirect co-culture. The fibroblasts were cultured in multiwell and felt the influence of melanocytes seeded on a transwell place inside the well of the multiwell. This influence is effective as in comparison the control the samples expressed $\alpha$ -SMA. ....	52
Figure 30: Analytic comparison of percentage of fluorescence positivity to $\alpha$ -SMA of the different conditions (number of total images n=35). The control shows no expression of $\alpha$ -SMA as expected, whereas the conditioned medium culture has a good expression, but the better condition for the development of fibroblast expressing $\alpha$ -SMA is the indirect co-culture. ....	53
Figure 31: Immunofluorescence comparison between dynamic and static culture of endothelial cells. a) Static culture. The endothelial cells proliferate in an anisotropic shape not showing any orientation and directionality. b) Dynamic culture. The endothelial cells subjected to dynamic flow tend to take a specific directionality and orientation following the flow lines. They also show an elliptic shape. ....	54
Figure 32: Histogram representation of cell directionality for endothelial cells cultured in a) dynamic condition and b) static condition. Imaging analysis operated with ImageJ on a total of images n=33. ....	55
Figure 33: The bar graph represents the roundness of endothelial cells, where 0 corresponds to completely flat cells and 1 to fully round cells. Cells cultured under static conditions exhibit significantly higher roundness compared to those in dynamic conditions suggesting that dynamic	

culture promotes a more elongated cell morphology. Error bars indicate standard deviation.

Number of total ROI investigated n=316. ....56

Figure 34: Immunofluorescence analysis of endothelial markers. (a) Cells cultured under dynamic conditions simulating the in vivo environment. (b) Cells cultured under static conditions. Endothelial markers are shown in red, while cell nuclei are stained with DAPI. ....57

Figure 35: Immunofluorescent images of HUVEC and Hff-1. a) 20 x shot of the sample. It gives a global indication of the behaviour of HUVEC with Hff-1. At 8 days co-culture the endothelial cells supported by the fibroblast begin a self-organization process in vasselike structures. This process is implemented in the 10 days co-culture. b) 60 x shot of the sample. Zoomed view of the vasselike structures where the ramification structure could be observed. ....58

Figure 36: Comparison of NP distribution on samples with vasselike structures and without. a) Sample with the presence of vasselike structures. With the passing of time, the NP diffuse inside the fibroblast hydrogel thanks to the presence of the vase structures formed by the HUVEC. b) Sample without the vasselike structures. In contrast with the other sample the NP do not diffuse easily inside the hydrogel as there are no vase structures. The dotted line represents the transwell membrane. ....59

# Table of contents

<b>1</b>	<b>INTRODUCTION.....</b>	<b>13</b>
1.1	Metastatic cutaneous melanoma .....	14
1.2	Melanoma microenvironment (MME) composition .....	17
1.3	Medical Treatment .....	18
1.4	Melanoma Models.....	20
1.4.1	Spheroids.....	20
1.4.2	Human skin equivalents .....	22
1.4.3	Melanoma-on-chip.....	23
1.5	Aim of the work.....	25
<b>2</b>	<b>MATERIALS .....</b>	<b>27</b>
<b>3</b>	<b>METHODS .....</b>	<b>28</b>
3.1	Dermal model: Hydrogel composition.....	28
3.1.1	Rheological Test.....	30
3.1.2	Hydrogel biocompatibility .....	30
3.1.3	Hydrogel degradation kinetic .....	31
3.1.4	Native ECM protein deposition .....	32
3.2	Epidermal Model .....	33
3.2.1	Epidermal model maturation .....	33
3.3	Melanoma model .....	34
3.4	Vascular network model .....	37
3.4.1	Endothelial layer development .....	37
3.4.2	Endothelial layer maturation.....	38
3.4.3	Vascularized dermal model .....	39
3.5	Statistical analysis.....	40
<b>4</b>	<b>RESULTS .....</b>	<b>41</b>
4.1	Dermal Model .....	41
4.1.1	Rheological Test.....	41

4.1.2	Cell Viability.....	43
4.1.3	Gel Degradation.....	44
4.1.4	Native ECM protein deposition .....	45
<b>4.2</b>	<b>Epidermal Model .....</b>	<b>47</b>
<b>4.3</b>	<b>Melanoma Model .....</b>	<b>48</b>
4.3.1	Tumour Propagation.....	48
4.3.2	Fibroblast and melanocytes interactions .....	49
4.3.3	$\alpha$ -SMA expression.....	51
<b>4.4</b>	<b>Vascularized model.....</b>	<b>54</b>
4.4.1	Endothelial Cells characterization .....	54
4.4.2	Vascularized Dermal model.....	57
4.4.3	Vascular network patency .....	59
<b>5</b>	<b>CONCLUSIONS.....</b>	<b>60</b>
<b>6</b>	<b>RINGRAZIAMENTI .....</b>	<b>63</b>
<b>7</b>	<b>BIBLIOGRAPHY.....</b>	<b>65</b>



# 1 Introduction

Skin is the largest vital organ in the human body. It accounts for about 15% of the body weight and it performs many essential functions, including protection against external physical, chemical, and biological hazards, as well as preventing excessive water loss from the body and playing a role in thermoregulation.[1], [2]

As shown in Figure 1, the skin is composed of three layers: the epidermis, the dermis, and subcutaneous tissue.[2], [3]

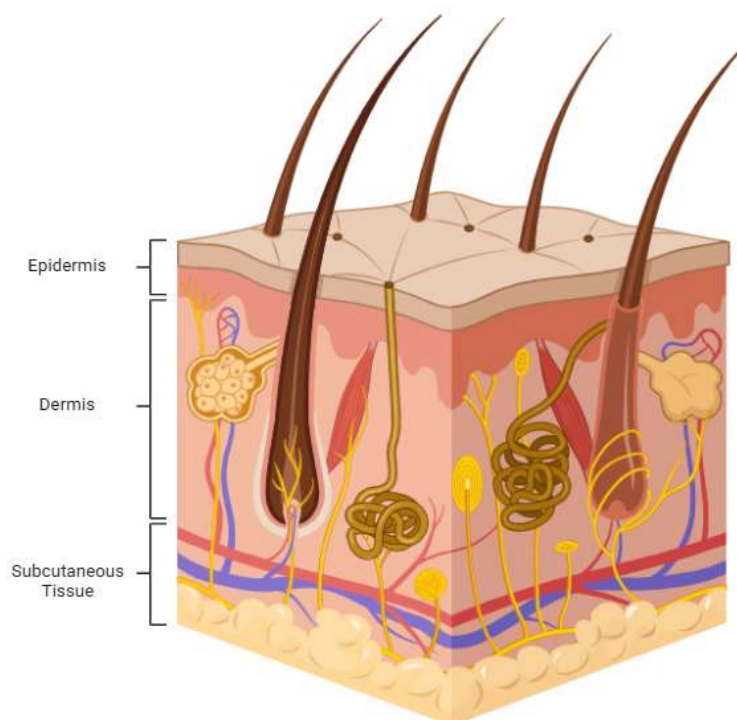


*Figure 1: structural anatomy of skin showing the three main layer: epidermis, dermis and the subcutaneous tissue. Illustration created with BioRender.com*

The epidermis is formed by a stratified squamous epithelium mainly composed of keratinocytes. [1], [2], [3], [4]

The epidermis presents a stratified structure composed by the squamous layer (stratum spinosum), which is 5-10 cells thick, responsible for the production of keratin, an insoluble protein that influences the architecture, mitotic activity, and cell signalling of epithelial cells. [1], [5] The granular layer (stratum granulosum) is located beneath the squamous layer. Here, keratinocytes present a flat

morphology, creating a more compact structure, which provides mechanical protection to the underlying epidermis and prevents water loss and invasion by foreign substances. [1], [2], [4]

The dermis lies under the epidermis and is connected to the epidermis by a basal membrane called the dermal-epidermal junction.[4]

The dermis is mainly populated by fibroblasts that preserve the structural integrity of the tissues and maintain a homeostasis. They deposit essential ECM proteins and release proteinases along with their inhibitors, thus balancing ECM production and degradation.[6], [7], [8], [9], [10] Other cell populations, including immune and inflammatory cells, as well as blood vessels and nerves, are present in the dermal stratum.[1], [4]

The dermal ECM is primarily composed of type I collagen, which accounts for the 75% of the dry skin weight. [11] It also contains other proteins, nerves, blood vessels, sweat glands and glycosaminoglycans (GAGs). Among GAGs, hyaluronic acid (HA) crosslinks with collagen, resulting in the formation of supramolecular structures and increasing tissue stiffness.[11]

The innermost layer of the skin is the hypodermis. It acts as a bridge between the dermis and deeper tissues such as muscles and bones. It contains subcutaneous fat cells, superficial fascia, blood vessels and nerves. This layer provides cushioning and thermal insulation.[1], [2], [4]

## **1.1 Metastatic cutaneous melanoma**

Metastatic melanoma (or stage IV melanoma) is one of the most aggressive forms of skin cancer, presenting extremely high mortality rate. According to the Global Cancer Observatory (GCO) 2018, an estimated 287,723 new cases of cutaneous melanoma were expected worldwide that year. The incidence of melanoma varies significantly across populations, with individuals of European origin being particularly affected. In these populations, the incidence rate stood at 11.2 cases per 100,000 people per year, with approximately 1.7 cases per 100,000 progressing to metastatic melanoma—a stage often leading to fatal outcomes. In the United States, the rates were slightly higher, at 12.2 cases per 100,000, with 1.4 cases being metastatic. The highest incidence was observed in Australia and New Zealand, where the strong sun exposure contributes to elevated melanoma rates. These regions reported 33.6 cases per 100,000 people annually, with 3.4 cases per 100,000 advancing to metastatic stages.[12], [13], [14], [15], [16]

Melanoma susceptibility is influenced by genetic and constitutional factors, such as race, gender, age, and number, size, and type of pigmented nevi, as well as by environmental factors, such as exposure to solar light. [12], [14], [17]

A 4-stage system for the classification of melanoma has been recommended by the American Joint Committee on Cancer (AJCC).[14] As explained in Figure 2, stage I and II represent the phases of localized tumour growth, when the pathology reaches the stage III an involvement of the surrounding tissue is present, and Stage IV indicates the development of systemic metastasis. [14]

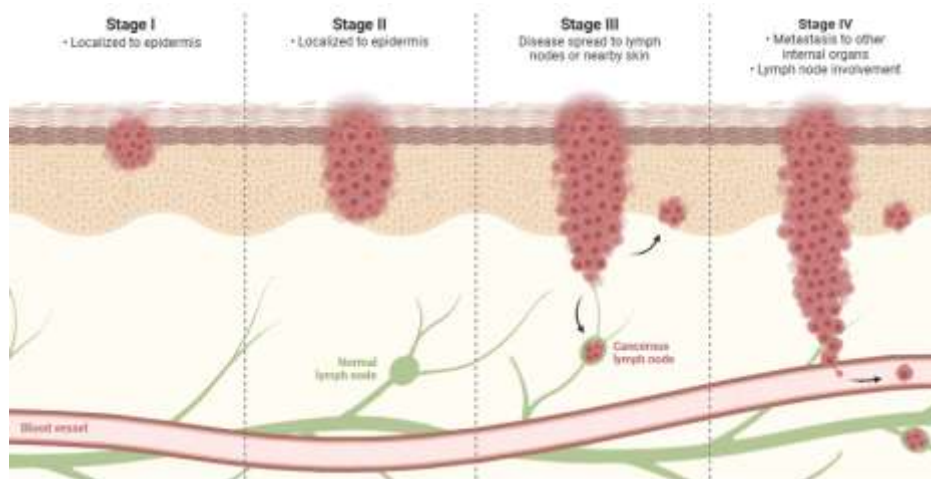


*Figure 2: Schematic representation of the progression stages of melanoma. Stage I present a localized melanoma. In Stage II there is cancer growth and cellular expansion. Stage III led to cellular spreading in the nearby tissues with the involvement of lymph nodes. Metastatic cells begin their spreading through the organism in stage IV. Illustration created with BioRender.com.*

The current WHO classification distinguishes four main types of melanomas: superficial spreading melanoma (SSM) (41%), nodular melanoma (NM) (16%), lentigo malignant melanoma (LMM) (2.7%-14%) and acral lentiginous melanoma (ALM) (1%- 5%). [13], [18]

SSM begins with an intraepidermal horizontal or radial growth phase, appearing first as a macular lesion that slowly evolves into a plaque. NM is a primarily nodular, often eroded or bleeding tumour, which is characterized by a predominant aggressive vertical growth phase. LMM is characterized histologically by a lentiginous proliferation of atypical melanocytes. ALM has typically a palmoplantar or subungual localization. In its initial intraepidermal phase there is irregular, poorly circumscribed pigmentation; later a vertical growth leads to a nodular component.[13], [14], [18]

The genesis of melanoma begins generally from an alteration of melanocytes functions.[16] With reference to Figure 3, in response to UV-radiation (UV-R) exposure, skin keratinocytes produce melanocyte-stimulating hormone (MSH) that binds melanocortin receptor 1 (MC1R) on melanocytes

resulting in the release of melanin to shield the underlying skin and to prevent DNA alteration.[12], [14] Sometimes this melanin-protection system might not be able to shield the DNA, leading to the development of melanoma. The genes that are commonly mutated in melanoma are BRAF, N-RAS, and NF-1 (Figure 3).[17], [19], [20], [21]

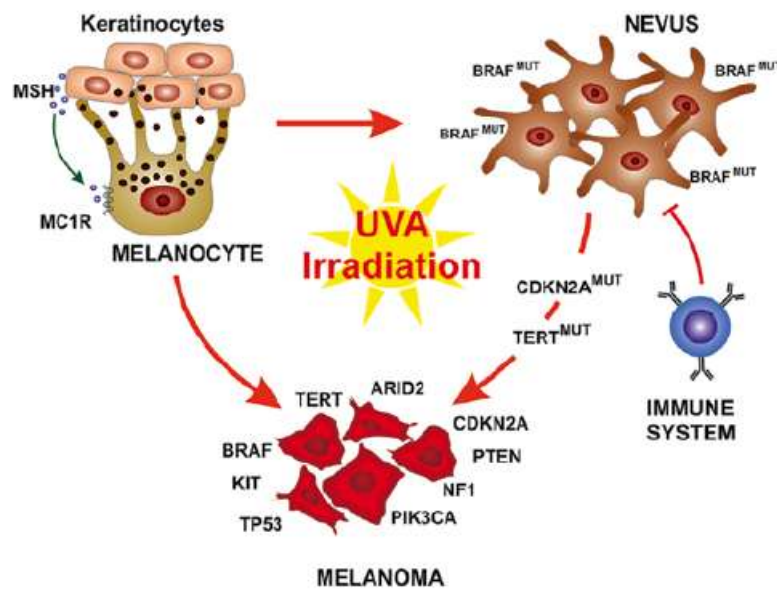


Figure 3: Schematic representation of melanoma genesis. Exposure to UV radiation triggers keratinocytes to send activation signals to melanocytes, stimulating melanin production. This pigment plays a crucial role in protecting melanocytes from UV-induced DNA damage. However, in some cases, this protective mechanism is insufficient, leading to DNA mutations in melanocytes. In the most severe cases, these mutations result in the transformation of melanocytes into melanoma cells. In other instances, mutated melanocytes develop into benign nevi cells, which, over time, may still acquire further mutations and progress into melanoma.[12]

Several studies indicated that mutations of the genes alter different pathways involved in melanocyte functions, such as MITF, KIT, snail/slugg, MAPK/ERK, and PI3K/AKT.[15], [22]

In particular, activation of the PI3K pathway is essential for melanoma progression, as it promotes cell proliferation, metabolism, motility, angiogenesis, and survival. [17], [19], [12], [15]

## 1.2 Melanoma microenvironment (MME) composition

Tumour malignancy and progression are highly related to its microenvironment, which is mainly constituted by fibroblasts, vascular endothelial cells, pericytes, adipose cells, lymphatic endothelial cells, and immune cells, together with the abundant extracellular matrix (ECM) (Figure 4).[6], [23]

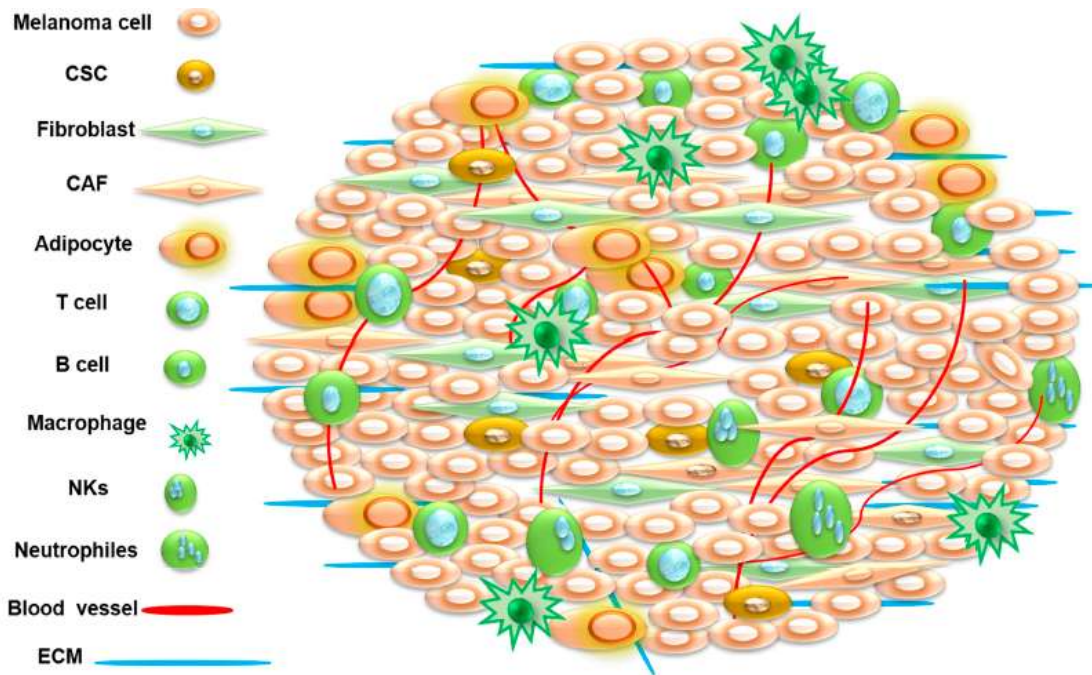


Figure 4: Schematic diagram of the tumour microenvironment. The tumour microenvironment is a complex ecosystem composed of heterogeneous components, including tumour cells, stromal cells, various types of immune cells, soluble molecules, and extracellular matrix (ECM) components.[53]

During tumour development, a constant inflammatory environment is present. This condition led to the activation of the fibroblast present in the MME. Activated fibroblasts, namely cancer associated fibroblasts (CAFs) contribute to tumour-promoting inflammation and fibrosis. They are a high proliferating subpopulation of fibroblasts presenting elongated morphology, that resides within or in proximity of the tumour mass.[6], [8], [9] Fibroblasts activation is initiated by the secreting of signalling molecules derived from tumour cells, in combination with autocrine signalling.[9], [24] CAFs express different markers in common with myofibroblast, the activated form of fibroblast associated with the wound healing process (e.g.  $\alpha$ -smooth muscle actin ( $\alpha$ -SMA)). [10], [24], [25], [26]

Even immune cells play a central role in MME. The immune system normally functions to constantly survey and eliminate pre-cancerous cells to prevent progression of melanoma.[25] On the onset of melanoma due to the high plasticity of tumour cells, a subset of transformed cells can acquire

properties that lead to immune evasion. These cells escape the elimination lead by the immune system and the proliferation of this subset brings to tumour progression.[25]

Considering the above, tumour microenvironment (TME) plays a crucial role in tumour malignancy and progression in different ways. CAFs contribute to tumour-promoting fibrosis, while tumour cells exploit immune system plasticity to escape surveillance. These dynamic interactions within the TME ultimately drive tumour development and progression.[23]

### **1.3 Medical Treatment**

For most of the patients with newly diagnosed melanoma the surgical excision represents the best treatment and is curative in most cases. However, there is a 10% of cases in which the pathology is diagnosed in an advanced stage, when the cancer is unresectable or already metastatic. [12]

Current literature highlights the lack of precise guidelines for optimal frontline treatment of melanoma. In general, treatment strategies vary depending on the tumour stage. As previously mentioned, surgical excision remains the standard of care, particularly in the early stages of the disease.[26] However, other options, such as radiotherapy, chemotherapy, and immunotherapy, may be employed. The selection of the most appropriate therapeutic approach depends on several factors, including tumour characteristics, disease progression, and individual patient considerations.[26]

Radiotherapy is rarely used for non-metastatic melanoma; it is often recommended for elderly patients when surgery could cause severe disfigurement. This treatment has shown effectiveness in controlling metastases, particularly in the skin, bones, and brain.[26], [27] However, a major limitation of radiotherapy is the exposure to radiation, which may increase the risk of developing other pathologies.[28]

The mostly exploited chemotherapeutic agent in melanoma treatment is dacarbazine, which is considered the standard of care for metastatic melanoma since 1972. Unfortunately, this drug presents important side effects, such as nausea, vomiting and myelosuppression. [27]

An innovative approach for the treatment of metastatic melanoma is immunotherapy, which is based on the enhancement of the body's immune system to fight diseases, including cancer, autoimmune disorders, and infections. [27] There are 4 main types of immunotherapies: biological immunotherapies, vaccination strategies, adoptive cells therapies and immune checkpoint inhibitors. Biological immunotherapy exploits high doses of interleukin-2 (IL-2), a crucial signalling glycoprotein

that plays a key role in immune system regulation. IL-2 promotes the survival, proliferation, and differentiation of T cells, essential components of the body's defence mechanisms. By stimulating T cells *in vivo*, IL-2 enhances their cytotoxic properties, enabling them to recognize and attack tumour cells more effectively. [27], [28], [29], [30]

Another promising strategy for the treatment of this pathology is represented by vaccines. The core principle behind this strategy is to identify antigens present on melanoma cells that can trigger a robust immune response. Once these antigens are introduced into the patient's system, they stimulate the activation of T cells to recognize and destroy malignant cells.[28]

Good results came from the use of adoptive cell therapy (ACT), although this is still at an experimental level and requires further validation before being considered a safe and efficacious strategy. ACT involves the collection of lymphocytes from the blood or tumour of the patient and their selection, expansion, and activation *in vitro*. The processed lymphocytes are then infused to the patient to induce an immune anticancer response.[28]

Immune checkpoint blockade is a form of immunotherapy designed to enhance the immune system's ability to fight cancer by targeting specific regulatory pathways in T-lymphocytes. These therapies work by inhibiting immune checkpoints, which normally act as brakes on the immune response, thereby restoring and amplifying anti-tumour activity. The anti-tumour response of T-lymphocytes occurs in two main stages. First, the T-cells recognize tumour-associated antigens. This is followed by the delivery of a co-stimulatory signal through B7 proteins, which leads to T-cell activation and proliferation. Once activated, another molecule called CTLA-4 binds to B7 proteins. Instead of stimulating T-lymphocytes, CTLA-4 provides inhibitory signals, acting as a negative feedback mechanism to regulate immune activity. Blocking this inhibitory checkpoint removes the suppression of T-cells, allowing them to sustain their anti-tumour activity. One example of this approach is ipilimumab, a human monoclonal antibody that targets CTLA-4. It has been approved for the treatment of metastatic melanoma and is undergoing further clinical trials for other types of cancer. [21], [28], [31]

## 1.4 Melanoma Models

As previously mentioned, tumour growth and its reaction to therapies are strongly shaped by the TME. The development of representative *in vitro* models able to accurately replicate melanoma TME is crucial to identify more effective treatments. Currently, preclinical melanoma models mainly rely on oversimplified 2D cell cultures or on animal models, which present different limitations.[32] 2D cell cultures are generally inefficient in replicating the complexity of the *in vivo* environment. The major drawback is the absence of the ECM, which plays a crucial role in modulating cell behaviour, signalling, and drug response. Without ECM interactions, these models fail to accurately mimic physiological conditions.[33] On the other hand, animal models, though widely used, present important ethical concerns and high costs. Moreover, the significant biological differences between species limit their ability to predict treatment responses in humans. Variations in immune system function, TME composition, and genetic makeup may reduce the translational relevance of such models.[34]

The limitations of traditional melanoma treatment and research models have driven scientific efforts toward the development of three-dimensional *in vitro* models. These advanced systems more accurately replicate the tumour microenvironment, offering valuable insights into melanoma progression and treatment responses. The *in vitro* models mainly involved in mimicking melanoma are spheroids, human skin equivalents, and melanoma-on-chip.[17], [32], [34]

### 1.4.1 Spheroids

Tumour-derived spheroids are cell aggregates with the potential to partially replicate the *in vivo* tumour architecture, cell-cell interactions, hypoxia, nutrient, pH, and soluble factor gradients, gene expression, and drug resistance development. [34], [35], [36], [37]

Recently, Farhoumand et al. exploited melanoma spheroids to evaluate the effects of Nebivolol, an anti-cancer drug commonly involved in melanoma treatment. The authors investigated various anti-tumour molecules and found that Nebivolol was the only one that significantly affected spheroid viability.[38]

They observed changes in the size and compactness of melanoma spheroids, revealing a concentration-dependent effect. (Figure 5). Additionally, the study evaluated the effect of Nebivolol on tumour cells cultured in a two-dimensional environment to determine whether differences in sensitivity and responsiveness were influenced by morphology. The results indicated a higher

sensitivity to the anticancer drug in the two-dimensional culture. This increased sensitivity was attributed to the simpler drug diffusion process in a two-dimensional setting. In contrast, *in vivo* conditions present a more complex tumour morphology that hinders drug penetration, preventing it from reaching all tumour cells effectively. This highlights the potential of melanoma spheroid models in providing physiologically relevant insights into drug efficacy, ultimately advancing melanoma treatment strategies. [37]

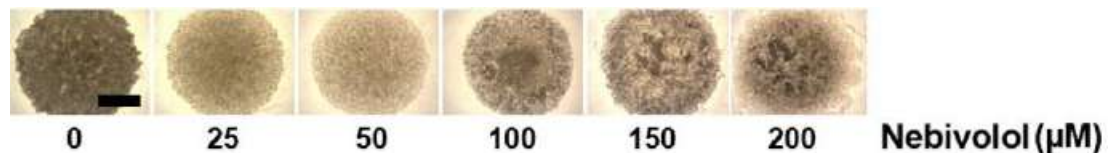


*Figure 5: Illustration of melanoma spheroids treated with different concentration of Nebivolol. As the drug concentration increases tumour cells presents a higher apoptotic behaviour. Cell viability seems to decrease already at 25 μM. [38]*

Spheroid models are valuable tools for replicating key characteristics of the melanoma tumour microenvironment (TME), but they have limitations that can affect their accuracy in mimicking *in vivo* conditions.

One of the primary challenges is the restricted diversity of cell types that can be co-cultured simultaneously. In a natural setting, the melanoma TME consists of a highly intricate network of interactions among various cell populations, including cancer-associated fibroblasts, immune cells, endothelial cells, and adipocytes, all embedded within the ECM. This complex interplay is crucial for tumour progression, immune evasion, and response to therapy.

However, accurately reproducing this environment in spheroid models remains a significant challenge. The inability to fully replicate such a dynamic system may impact the reliability of preclinical validation, potentially influencing the effectiveness of therapeutic testing and drug development.[17]

### 1.4.2 Human skin equivalents

While tumour spheroids serve as a useful 3D *in vitro* model for mimicking tumour structure, they fall short in replicating the native cellular organization. In fact, they lack of epidermal and dermal components, which are key factors that influence the invasiveness and aggressiveness of melanoma.[17], [34]

Human three-dimensional *in vitro* skin equivalents (HSE) can partially overcome these limitations. They are bioengineered substitutes of skin built using human skin cells (keratinocytes, melanocytes and fibroblast) and component of the ECM (mainly collagen) specifically designed to study cell-type specific epithelial-stromal interactions. [34], [39], [40]

As shown in Figure 6, these models present a stratified structure that closely replicates the complexity of human skin.[41]

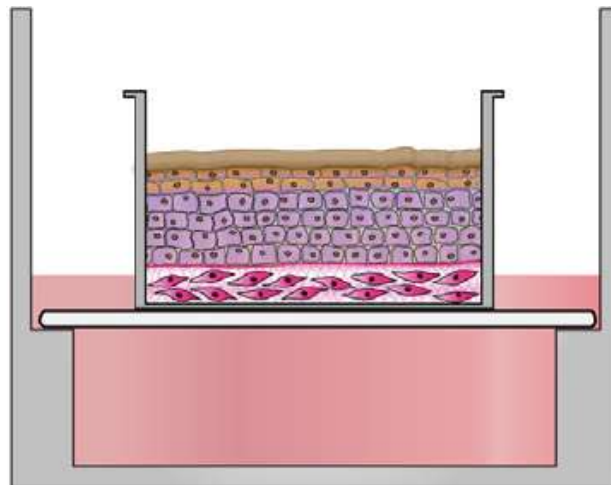


*Figure 6: Schematic representation of the HSE. The bottom layer presents the dermal compartment composed by fibroblast seeded hydrogel. On top of that there is the epidermis model composed of keratinocytes seeded on top of the dermal model, matured on correspondence of air-liquid interface.[41]*

The key advantage of the HSE is its ability to integrate tumour cells, like melanoma cells, into a complex structure which effectively recreates the architecture of the native tissue. This makes it a highly effective tool for studying tumour progression and invasion, as well as a valuable system for pharmacological analyses.[34] Haridas et al. utilized HSE to examine the proliferation, migration, and invasiveness of melanoma cells. Their study involved seeding melanoma cells onto a fully matured HSE model to observe their behaviour in a controlled environment. The results demonstrated that melanoma cells not only proliferated within the model but also actively migrated from the epidermis

into the dermis, exhibiting their capability to colonize the surrounding tissue. Figure 7 illustrates the behaviour of melanoma cells over 0, 9, 15, and 20 days. Initially, melanoma cells were confined to the epidermal layer (Figure 7a). However, as time progresses, they began to invade the underlying dermis (Figures 7b–7c). By day 20 (Figure 7d), melanoma was well established within the dermal layer, demonstrating the ability of melanoma cells to proliferate, migrate, and invade surrounding tissues. These findings underscored the potential of Human Skin Equivalent (HSE) models in enhancing the understanding of melanoma progression and metastasis. [41]

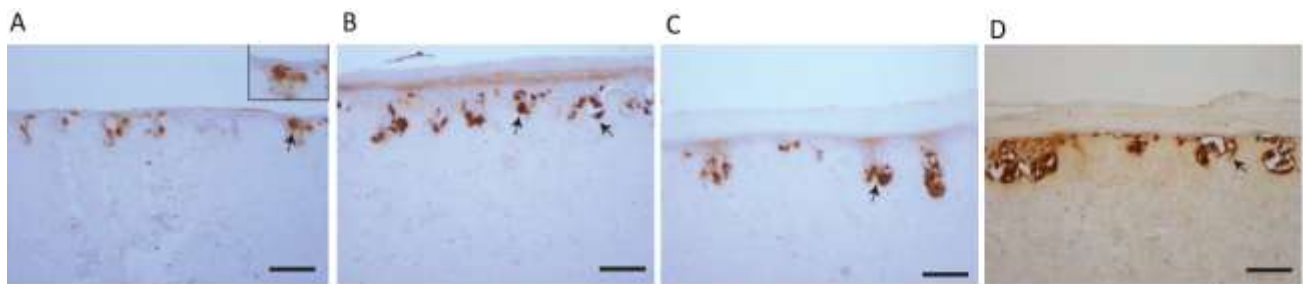


Figure 7: Proliferation, migration and invasiveness of melanocytes in an HSE at 0, 9, 15, 20 days. Black arrows and inset images highlight positive staining. The scale bar in the main images shows 100  $\mu$ m, and the width of the insets are approximately 75  $\mu$ m.[42]

Although human skin equivalents (HSEs) are widely used as organotypic models, their development presents several technical challenges. Key difficulties include selecting a suitable extracellular matrix, optimizing cell densities, formulating effective culture media, and maintaining proper air-liquid interface conditions. Additionally, ensuring accurate post-culture analysis remains a critical hurdle. Finally, the big obstacle in using this model is the absence of a dynamic environment able to mimic the complex microvascular system of the skin. Overcoming these challenges is essential for improving the reliability and reproducibility of HSE models in research and clinical applications. Continued advancements in tissue engineering and biomaterials are crucial for refining these constructs and enhancing their effectiveness in biomedical studies.[34]

### 1.4.3 Melanoma-on-chip

Organ-on-chip based models exploit microfluidic devices to replicate key physiological functions of human organs by culturing living cells within a dynamic environment. These models integrate fluid flow, mechanical cues, and multicellular interactions to better mimic the complexity of *in vivo* conditions compared to traditional 2D or 3D culture systems.[34], [43] The involvement of microfluidic platforms allow the culture of living cells in micrometre-sized chambers with continuous

infusion, enabling the controlled release of growth factors and nutrients. Furthermore, the microscale approach makes these platforms highly cost-effective for drug screening applications.[36], [46], [47] This technology accurately recreates the melanoma microenvironment by embedding melanoma cells within the model as spheroids or organoids. These structures are co-cultured with key stromal cells, including keratinocytes, fibroblasts, immune cells, and endothelial cells. This approach enables a comprehensive investigation of melanoma TME interactions, offering valuable insights into tumour progression and therapeutic responses.[44]

A notable example is the study by Ayuso et al., in which the authors developed a model where melanoma cells and stromal cells were seeded into separate chambers connected by narrow channels. This setup demonstrated the significant influence of stromal cells, as fibroblasts and keratinocytes, on melanoma cell morphology, growth, metabolic phenotypes, and chemokine secretion. After cell seeding and attachment, cell behaviour was observed through fluorescence microscopy for up to three days. The results showed that approximately 90% of the cells remained viable and continued to proliferate. Melanoma cells exhibited the highest proliferation rate and displayed distinct morphological differences compared to those in two-dimensional culture. Notably, melanoma cells in this model adopted an elongated morphology, in contrast to the rounded shape typically seen in two-dimensional cultures.[45]

Herreros et al. reported the development of an innovative melanoma-on-chip platform based on the co-culture of primary fibroblasts, keratinocytes, and melanocytes (Figure 8). This system was designed to evaluate the effects of Gemcitabine on melanoma cell proliferation within a continuously perfused environment. Specifically, after seeding the three different cell lines, the culture was maintained for three days to allow for cellular attachment, proliferation, and stabilization in two separate chips. After three days, the anticancer drug was injected into one of the two chips, while the other served as a control. Following a three-hour incubation period, the results revealed a pronounced increase in cell death in the treated samples, whereas the untreated samples remained viable. This demonstrated the successful development of a reliable melanoma-on-chip able to mimic *in vivo* melanoma and that could be used for the test of anticancer drugs. [46]

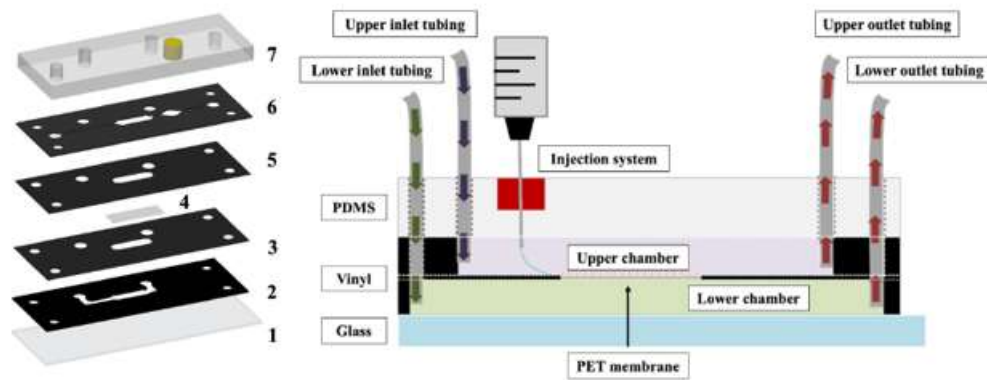


Figure 8: Exploded view of a melanoma on chip device and its flow diagram scheme, representing the volume injection procedure.[46]

Despite the advancements brought by microfluidic chips, the current state of the art still presents certain limitations. While these devices are designed to provide precise regulation and control of the TME, integrating *in situ* sensors remains difficult. Additionally, chip production is still largely manual, relying on laboratory PDMS. This is due to the absence of a standardized, high-throughput, and cost-effective manufacturing process, which limits scalability and broader application. Overcoming these limitations will be crucial for the broader adoption of microfluidic technologies in cancer research.[43]

## 1.5 Aim of the work

Literature highlights the difficulty of creating a vascular network in the model, and that the available models fall short in faithfully replicating the metastatic behaviour of melanoma.

The goal of this study is to develop a system able to reproduce the *in vivo* condition of a metastatic melanoma. To this aim, a custom-made microfluidic chip will be designed to host a multi-compartment model. The device will be composed by three chambers connected in series. The first chamber will allocate the primary melanoma model, while the other chamber will contain different matrices mimicking the mechanical properties of the tissues typically metastasized by melanoma (e.g. lung, brain, bone).

The primary melanoma model will integrate multiple cell types, including fibroblasts (Hff-1), melanoma cells (SK-MEL), endothelial cells (HUVEC), and keratinocytes (HaCaT), to create a biologically relevant microenvironment.

The dermal model will be realized with a collagen - methacrylated hyaluronic acid (Col-HAMA) gel, seeded with human dermal fibroblasts (Hff-1), which play a crucial role in ECM secretion. A spheroid of SK-MEL will then be incorporated in the dermal gel to mimic the presence of the tumour mass. Concurrently, a keratinocyte (HaCaT) layer will be seeded on top of the gel to recreate the epidermis, completing the multi-layer architecture of the skin. After that this model will be placed inside a endothelial cells (HUVEC) pre-culture transwell. HUVEC cells will be cultured on the bottom side of a transwell that, once flipped, will host the melanoma model. The HUVEC will enable the formation of vase-like structures inside the hydrogel, thus creating a vascularized melanoma model.

Placed the model inside the transwell, the entire system will be allocated inside a microfluidic chip. The employment of a microfluidic device permits the induction of dynamic culture which better replicate *in vivo* physiological conditions, such as nutrient flow, waste removal, and mechanical stimulation, essential for the development of the vascular network. In addition, these mechanical factors are critical for maintaining cellular functionality and communication *in vivo*. (Figure 9)

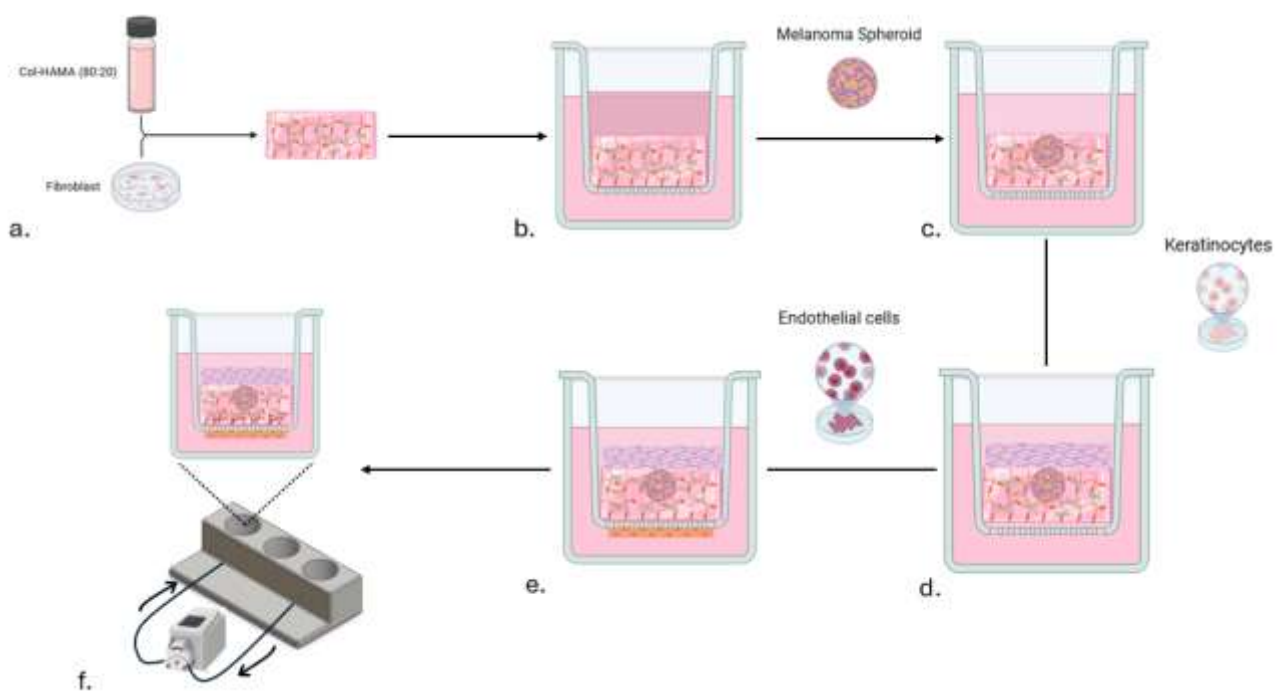


Figure 9: Schematic representation of the primary tumour model assembly. a) seeding of Hff-1 cells inside the Col-HAMA gel to produce the dermal model. b) Positioning of the dermal model inside a transwell. c) Installing of the melanoma spheroid inside the dermal model for the creation of the tumour model. d) Seeding of keratinocytes on top of the dermal layer to mimic the epidermal model. e) Seeding of endothelial cells on the bottom side of the transwell membrane to mimic the vascular system. f) Introduction of the system in the microfluidic chip to assure the dynamic condition. Illustration created with BioRender.com

The obtained 3D melanoma model hopefully will provide a physiologically relevant environment for studying tumour progression in a more ethical and cost-effective way.

Future developments include the optimization of the metastatic compartment and the employment of the model as a validation platform for innovative drug-delivery systems.

## 2 Materials

The supportive hydrogel used as dermal model were developed with Bovine Collagen Type I (Col) 10 mg/ml, Bovine Collagen Type I Methacrylate (ColMA) 10 mg/ml, Hyaluronic acid (HA) 10 mg/ml and Hyaluronic acid Methacrylate (HAMA) 10 mg/ml. The photoreticulation process was possible thanks to the combination of Lithium phenyl-2,4,6-trimethylbenzoylphosphinate (LAP) 1 mg/ml and visible light at 405 nm.

In this study, four distinct cell lines were utilized: human foreskin fibroblasts (Hff-1), derived from pooled foreskin samples of two individuals; the human melanoma cell line (SK-MEL), isolated from the skin of a 51-year-old male patient diagnosed with malignant melanoma; human umbilical vein endothelial cells (HUVEC), obtained from the umbilical cord vein; and spontaneously transformed human keratinocytes (HaCaT).

For 2D monolayer cultures, cells were maintained in tissue culture flasks (Jet Biofil®) and incubated at 37 °C in a humidified atmosphere containing 5% CO<sub>2</sub> (Thermo Scientific™ Heracell™ 150i CO<sub>2</sub> Incubator). Cell passaging was performed approximately every 72 hours, upon reaching 80–90% confluence, using Trypsin (Gibco™) to ensure efficient detachment and prevent overgrowth.

Hff-1 cell line was grown in Gibco™ Dulbecco's Modified Eagle Medium (DMEM) supplemented with 15% fetal bovine serum (FBS, Gibco™), 1% penicillin/streptomycin (Gibco™) and 2% L-Glutamine (Gibco™).

SK-MEL-28 cells were cultured in Roswell Park Memorial Institute (RPMI) 1640 Medium (Gibco™) supplemented with 10% fetal bovine serum (FBS, Gibco™), 1% penicillin/streptomycin (Gibco™) and 2% L-Glutamine (Gibco™).

HUVEC cells were cultured in Innoptot™ Dulbecco's Endothelial Cell medium (ECM) supplemented with 5% fetal bovine serum (FBS, Gibco™), 1% penicillin/streptomycin (Gibco™) and 1% of endothelial cell growth supplement ( Innoptot™).

HaCaT cells HUVEC cells were cultured in Gibco™ Dulbecco's Modified Eagle Medium (DMEM) supplemented with 10% fetal bovine serum (FBS, Gibco™), 1% penicillin/streptomycin (Gibco™) and 2% L-Glutamine (Gibco™).

To enhance the model and provide a dynamic culture environment, a three-chamber microfluidic chip was integrated into the system. This chip was connected to a pump that facilitated continuous medium flow, ensuring optimal conditions for cell growing.

### 3 Methods

#### 3.1 Dermal model: Hydrogel composition

The skin is composed of approximately 75% Collagen I, with the remaining 25% consisting of other proteins, nerves, blood vessels, sweat glands and most importantly glycosaminoglycans GAGs. Among the GAGs, HA play a crucial role in creating optimal mechanic conditions for the cellular components. By crosslinking with collagen, HA contributes to the stiffness and structural integrity of the skin.[11] To mimic dermal ECM, two different hydrogels compositions were investigated, as described in table 1:

- I. Bovine Collagen type I (Col) 10 mg/ml, Methacrylated Bovine Collagen type I (ColMA) 10 mg/ml and Methacrylated Hyaluronic Acid (HAMA) 10 mg/ml at a 40:40:20 ratio.
- II. Bovine Collagen type I (Col) 10 mg/ml, Methacrylated Hyaluronic Acid (HAMA) 10 mg/ml at 80:20 ratio.

<p>a)</p> <p><b>Col-ColMA-HAMA (40:40:20)</b></p> 	<ul style="list-style-type: none"> <li>• Bovine Collagene type I 40%</li> <li>• Bovine Collagene type I metacrilated 40%</li> <li>• Hyaluonic Acid metacrilated 20%</li> </ul>	<ul style="list-style-type: none"> <li>• High presence of methacrilated groups</li> <li>• High cost</li> <li>• Low cytocompatibility</li> <li>• Good mechanical characteristics</li> </ul>
<p>b)</p> <p><b>Col-HAMA (80:20)</b></p> 	<ul style="list-style-type: none"> <li>• Bovine Collagene type I 80%</li> <li>• Hyaluonic Acid metacrilated 20%</li> </ul>	<ul style="list-style-type: none"> <li>• High cost</li> <li>• Good cytocompatibility</li> <li>• Good mechanical characteristics</li> </ul>

**Table 1:** (a) Col-ColMA-HAMA (40:40:20) – After the reticulation process, this formulation achieves high stiffness due to the abundance of methacrylated groups. However, this may result in lower cytocompatibility and increased costs. (b) Col-HAMA (80:20) The high collagen content leads to increased costs, but this formulation offers excellent cytocompatibility and favourable mechanical properties.

To prepare the dermal hydrogel, collagen was solubilized at a concentration of 10 mg/ml in 0.5 M acetic acid solution in culture medium. The solution was then stirred magnetically at 400 rpm at 4°C overnight to prevent gelation.

The following day, 1 M NaOH was added to the collagen solution to neutralize the pH. The same protocol was followed for the ColMA solution.

Simultaneously, the HAMA solutions were prepared. This solution was obtained by dissolving HAMA in culture medium at a concentration of 10 mg/ml. This mixture was then stirred magnetically at 500 rpm at 20°C for 4 hours.

The final formulations were assembled according to the previously defined proportions and fibroblasts were added at a concentration of 1,000,000 cells/ml. The photo-initiator Lithium phenyl-2,4,6-trimethylbenzoylphosphinate (LAP) at a concentration of 1 mg/ml was added.

To induce the crosslinking of the hydrogels, the samples were firstly exposed to visible light (405 nm) for 60 second, subsequently thermal crosslinking was obtained by incubating the hydrogel at 37 °C for 30 minutes to induce collagen fibrillogenesis. (Figure 10)

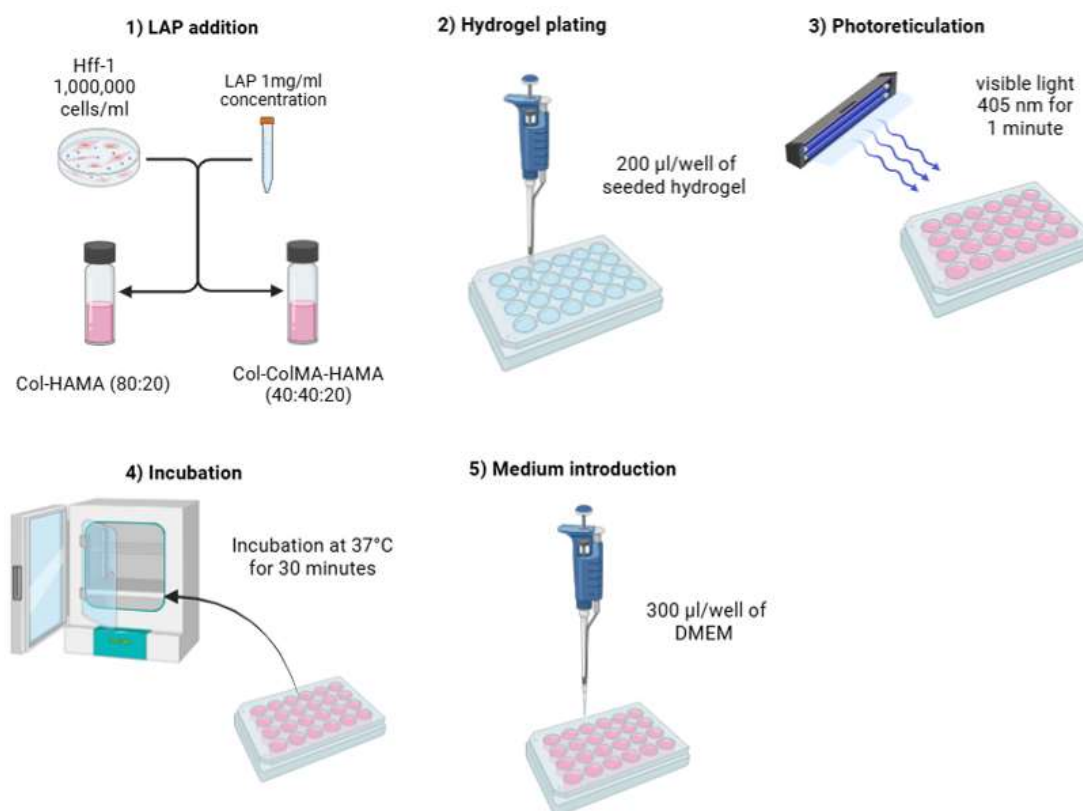


Figure 10: Schematic illustration of the reticulation process of both Col-HAMA (80:20) and Col-ColMA-HAMA (40:40:20) formulations. Illustration created with BioRender.com

### **3.1.1 Rheological Test**

Rheological tests were conducted on two different formulations: Col-CoIMA-HAMA (40:40:20) and Col-HAMA (80:20).

The formulations were prepared as previously described without embedding fibroblasts.

A time sweep test was conducted to analyse the evolution of the storage modulus ( $G'$ ), which reflects the gel's elastic behaviour, and the loss modulus ( $G''$ ), which provides insights into its viscous behaviour, throughout the crosslinking process. The test lasted 30 minutes, during which the samples were initially irradiated with 405 nm visible light for 60 seconds at room temperature. Subsequently, they were maintained at 37°C to induce collagen crosslinking. To prevent sample dehydration, a solvent trap was placed at the sample borders throughout the experiment.

Once the samples were fully crosslinked, their mechanical behaviour under different strain levels was investigated through a strain sweep test. This test is a fundamental rheological method used to characterize the mechanical properties of viscoelastic materials, such as gels, hydrogels, and polymers. Specifically, it provides critical information about the material's response to increasing deformation and helps determine the linear viscoelastic region (LVR), as well as the flow point ( $\gamma_f$ ), the strain threshold beyond which the gel transitions into a liquid state. The test was performed at room temperature, covering a strain range from 0.01% to 1000%, while ensuring sample integrity by maintaining the previously mentioned solvent trap.

### **3.1.2 Hydrogel biocompatibility**

To identify the optimal hydrogel composition, cell viability quantification was performed at different timepoints. Cell viability was assessed on two hydrogel compositions: Col – CoIMA – HAMA and Col – HAMA.

Hff-1 were seeded within the hydrogel and cultured for up to 21 days. Cell viability was quantified every 7 days, via CellTiter-Blue<sup>®</sup> cell viability assay (Promega), which measures ATP levels as an indicator of viable cells. This assay is non-toxic, allowing repeated measurements on the same samples over time without compromising cell integrity.

At each time point, the culture medium was removed and replaced with 150  $\mu$ L of CellTiter-Blue assay solution, prepared at a 1:6 ratio in cell culture media. The samples were incubated for three hours, after which the assay solution was collected for fluorescence measurement. Fresh culture medium was added to the wells following the assay.

For each time point, three replicates per hydrogel formulation were prepared, as previously described, in a 48-well multiwell plate using 200  $\mu\text{L}$ /well.

Following crosslinking, the samples were maintained at 37°C in 200  $\mu\text{L}$ /well of DMEM. Once the specific time point was reached, the protocol for CellTiter-Blue assay was followed.

### 3.1.3 Hydrogel degradation kinetic

To evaluate the degradation kinetic of the Col-HAMA (80:20) hydrogel, hydrolytic degradation tests were conducted.

For this experiment, 1.5 ml Eppendorf tubes were used, with each tube weighed beforehand to record the tare weight. 200  $\mu\text{L}$  of COL – HAMA hydrogel, prepared as previously described, was poured into each Eppendorf tube, followed by crosslinking. After crosslinking, the samples were weighed, 300  $\mu\text{L}$  of ultra-pure distilled water (ddH<sub>2</sub>O) were added to the samples and incubated at 37 °C. At specified timepoints (3, 24, 48, 72 hours, and 7 days), samples were collected, weighed following the removal of residual ddH<sub>2</sub>O, subjected to lyophilization, and weighed again. The experiment was performed in triplicate. The wet weight variation % and the dry weight variation were obtained respectively through Equation 1 and Equation 2:

$$\text{Wet Weight variation (\%)} = \frac{W_{t_i,w}}{W_{0,w}} \times 100 \quad (1)$$

$$\text{Dry Weight Variation (\%)} = \frac{W_{t_i,d}}{W_{0,d}} \times 100 \quad (2)$$

where:

- $W_{t_i,w}$  is the weight of the wet formulation at the specific time point;
- $W_{0,w}$  is the weight of the wet formulation at the initial time point;
- $W_{t_i,d}$  is the weight of the dry formulation at the specific time point;
- $W_{0,d}$  is the weight of the dry formulation at the initial timepoint.

Figure 11 is an illustration of the protocol.

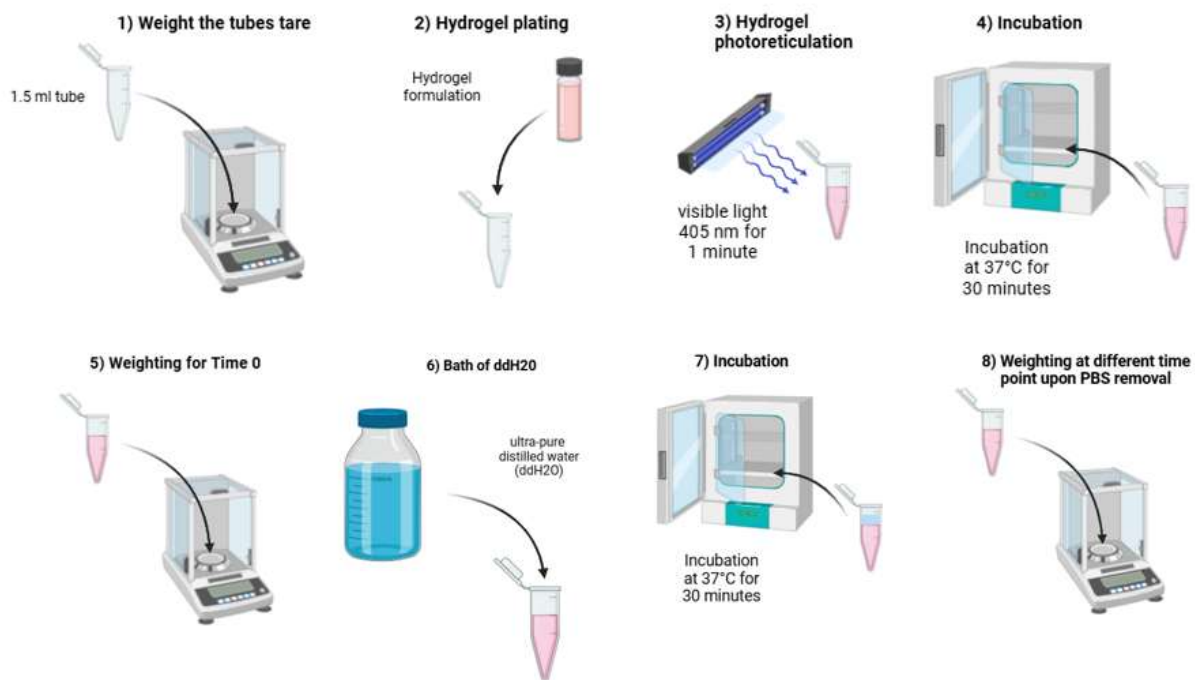


Figure 11: Schematic representation of the protocol for the derivation of the wet degradation data of the Col-HAMA (80:20) hydrogel. Illustration created with BioRender.com

### 3.1.4 Native ECM protein deposition

Fibroblasts play a well-established homeostatic role in the extracellular matrix (ECM), regulating the production of proteins such as collagen and fibronectin.[49]

To evaluate the capability of Hff-1 to secrete native dermal ECM protein when cultured within the COL – HAMA matrix, the hydrogel was prepared as previously described and the deposition of human collagen type I and human fibronectin was analysed through immunofluorescence at different timepoints (0, 7, 14, 21 days).

Fibroblasts cultured in the 3D matrix were fixed with 4% paraformaldehyde (PFA), followed by permeabilization with 0.5% Triton X-100 and blocking for 45 minutes in Thermo Scientific™ SuperBlock™ Blocking Buffer. The gels were then incubated overnight with Anti-Collagen Type I Mouse polyclonal Antibody (Cell Signaling Technology, E3E1X, 1:100 dilution) and Anti-Fibronectin Rabbit monoclonal Antibody (Cell Signaling Technology, E5H6X, 1:100 dilution). Secondary antibodies used for immunostaining included Goat Anti-Rabbit IgG H&L Alexa Fluor® 555 (Abcam, AB150078, 1:200 dilution) and Goat Anti-Mouse IgG H&L Cross Adsorbed (Invitrogen, A10524, 1:200 dilution). The incubation with the secondary antibody was 1 hour. Counterstaining for

nuclei and F-actin filaments was performed by incubating samples with 4',6-Diamidino-2-phenylindole (DAPI)/phalloidin following manufacturers' protocols.

## **3.2 Epidermal Model**

The skin plays a crucial role in protecting the human body, acting as a barrier that separates the internal environment from the external world. The outermost layer consists predominantly of keratinocytes forming a thick, protective barrier that is continuously exposed to the air.[1], [2] This unique "air/liquid" interface is a defining characteristic of the skin and a critical aspect to consider in any in vitro model aiming to replicate its functions.[41]

### **3.2.1 Epidermal model maturation**

Firstly, the dermal model was prepared as previously described and incubated for 14 days at 37°C in a 24-well transwell system using DMEM medium supplemented with 15% FBS, 1% P/S and 2% L-glu. After this incubation period, keratinocytes (HaCaT) were seeded on the top surface of the Col-HAMA hydrogel at a concentration of 200,000 cells/cm<sup>2</sup> and incubated at 37°C, with the medium covering the top layer to allow keratinocyte adhesion and proliferation.

Following 4 days of incubation, the culture medium was removed from the apical compartment of the transwell to establish the cell culture at the air-liquid interface. The system was then incubated at 37°C and analysed after 7 days and 10 days. The experiments were performed in duplicate. Figure 13 is a schematic representation of the epidermal model creation process.

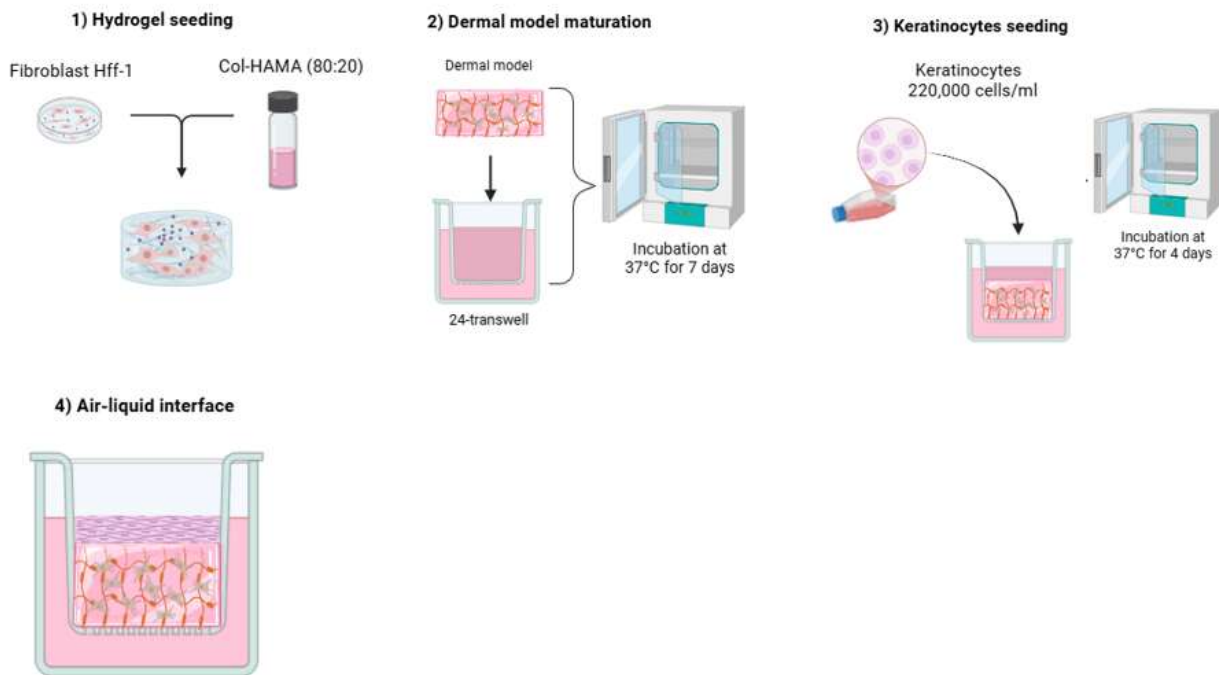


*Figure 12: Schematic representation of the step toward the creation of the epidermal model. After the 7 days maturation of the dermal model, a layer of keratinocytes was placed on top of the Col-HAMA hydrogel and incubated for 4 days in medium. Then the medium on top of the layer was removed to create the air-liquid interface typical of in vivo skin. Illustration created with BioRender.com*

To observe the establishment and the maturation of the epidermal layer on top of the dermal model, immunostaining for Cytokeratin, a protein found in the cytoskeleton of epithelial cells [50], was performed. The samples were fixed with 4% PFA, followed by permeabilization with 0.5% Triton X-100 and blocking for 45 minutes with Thermo Scientific™ SuperBlock™ Blocking Buffer. The gels were then incubated with Anti-Cytokeratin 14 antibody [SP53] (Abcam, ab119695, Rabbit, 1:234 dilution) overnight. After that the samples were incubated with Goat Anti-Rabbit IgG H&L Alexa Fluor® 555 (Abcam, AB150078, 1:200 dilution) for 1 hours. Nuclei and actin filaments were stained with DAPI and phalloidin, respectively.

### 3.3 Melanoma model

The dermal model was developed following the previously established protocols and maintained in DMEM supplemented with 15% FBS at 37°C for 14 days. Subsequently, one tumour spheroid of melanoma cells (SK-MEL 28) was introduced into the gel, and its behaviour observed.

To prepare the tumour spheroids, SK-MEL 28 cells were cultured in 96-well ultra-low attachment plates (U-multiwell) at a concentration of 40,000 cells/ml in 100 µl of RPMI medium 10% FBS, 1% P/S, 2% L-glu for three days to allow spheroid formation.

Spheroids were incorporated into the collagen-based hydrogel manually. The samples were kept in culture for up to 10 days at 37°C in a medium mixture of DMEM and RPMI 50:50. (Figure 14)

Two different conditions were investigated: i) SK-MEL spheroid single culture and ii) SK-MEL spheroids in co-culture with Hff-1. SK-MEL spheroids behaviour was observed at different time point of 0, 1, 4, 7, and 10 days through optical microscopy

Immunofluorescent staining for Human Collagen I and Fibronectin was performed as already described.

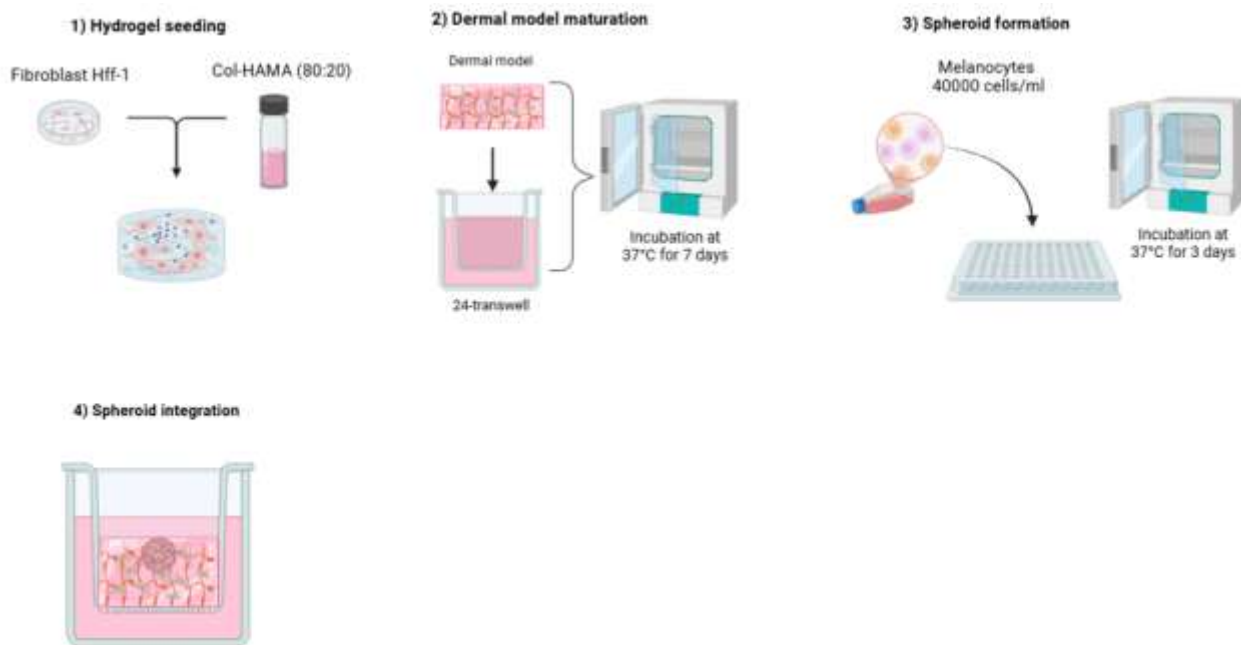


*Figure 13: Schematic representation of the procedure to obtain the melanoma model. The key procedure is the integration of a SK-MEL spheroid within the dermal model. Illustration created with BioRender.com*

The expression of MLAN-A, a protein involved in the process of production and transportation of melanin by melanoma cells was also assessed by immunofluorescence [51] after overnight incubation with MLANA/MART-1 Rabbit mAb (Cell Signaling Technology, E9Q40, 1:800 dilution).

To investigate the activation of Hff-1 into a cancer-associated fibroblast (CAF) phenotype, expression of Alpha Smooth Muscle Actin ( $\alpha$ SMA) was evaluated through immunofluorescence analysis. Hff-1 were cultured in different conditions: i) indirect co-culture of melanocytes and fibroblasts in cell culture inserts, ii) culture of fibroblasts with melanocyte-conditioned medium (MCM) (96 h).

Specifically, to perform indirect co-culture approach, Hff-1 fibroblasts were seeded in 24-well plates in RPMI at a concentration of 50,000 cells/well, while SK-MEL cells were simultaneously seeded in 12 mm transwells at a concentration of 100,000 cells/well. After 24 hours, the transwells were placed into the multiwell plates containing Hff-1, and the co-culture was maintained for seven days. (Figure 15)

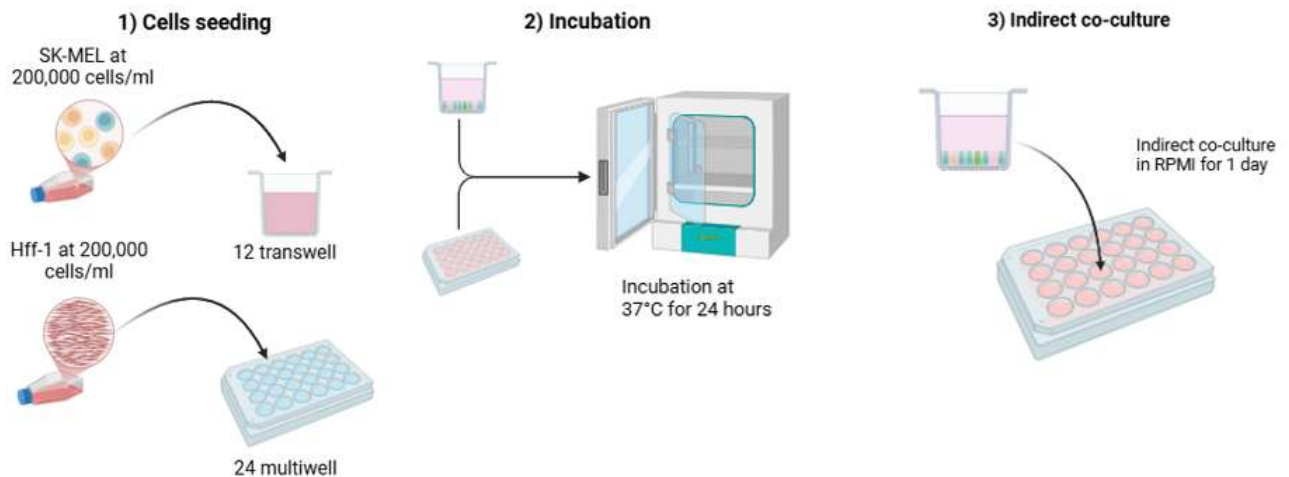


*Figure 14: Illustration of the indirect co-culture protocol. Hff-1 and SK-MEL cells were seeded simultaneously in separate flasks. Once they reached confluence, they were transferred to a well of a 24-well plate and a Transwell insert, respectively. After 1 day of culture, the Transwell insert was placed into the multiwell, and the system was incubated for an additional day. Illustration created with BioRender.com*

In the second approach, fibroblasts were seeded in 48-well plates at a concentration of 200,000 cells/ml and cultured for 7 days under two medium conditions: RPMI (control), and RPMI (MCM). Each condition was performed in triplicate. (Figure 16)

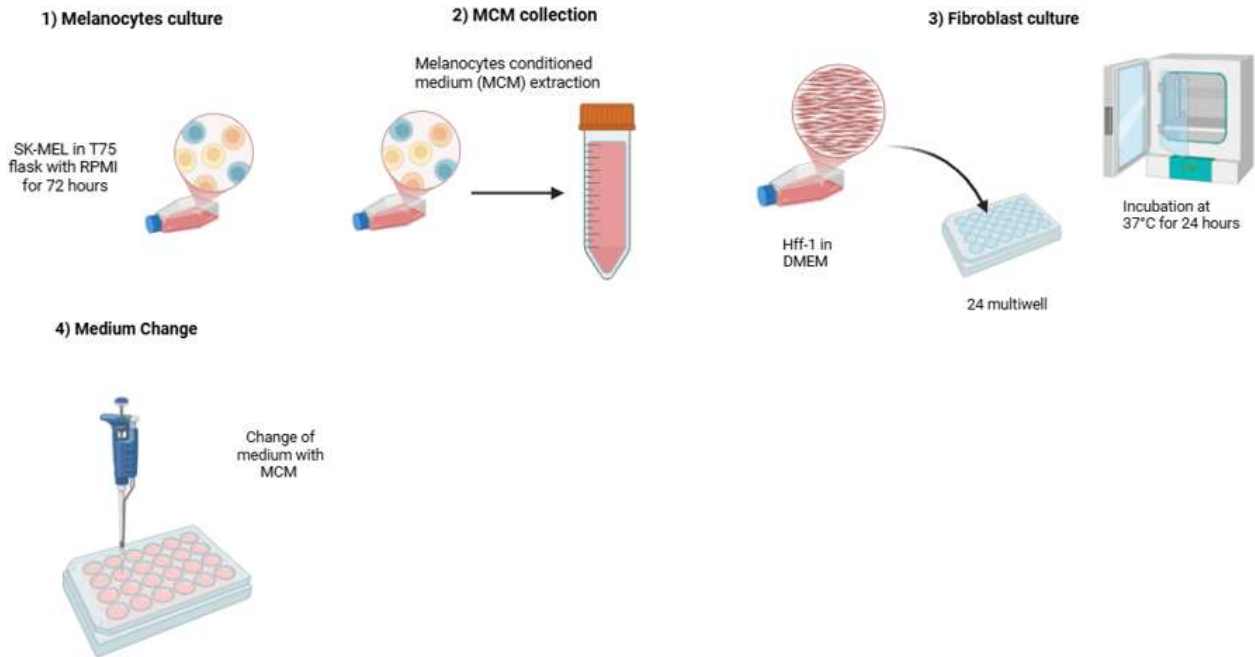


Figure 15: Illustration of the melanoma conditioned medium protocol. Conditioned medium is withdrawn from a melanocytes-seeded flask. Hff-1 were incubated under normal RPMI (CTRL) and conditioned RPMI. Illustration created with BioRender.com

To evaluate fibroblast activation into a CAF-like phenotype, immunofluorescent staining for alpha-smooth muscle actin ( $\alpha$ -SMA) was performed as previously described, using a primary recombinant Monoclonal Anti-Actin, Smooth Muscle Clone (Sigma-Aldrich, CGA7, Mouse, 1:100 dilution) antibody. A secondary antibody, Goat Anti-Mouse IgG H&L Cross Adsorbed (Invitrogen, A10524, 1:200 dilution), was applied and incubated 1 hour to complete the staining process

### 3.4 Vascular network model

#### 3.4.1 Endothelial layer development

The development of a physiologically relevant skin model requires the establishment of a basal layer composed of endothelial cells. To achieve this, HUVEC cells were cultured on the basal compartment of the transwell membrane. Initially, to favour endothelial cells adhesion, a collagen coating was applied on the surface of the membrane and incubated for 1 hour at 37°C. Endothelial cells were seeded onto the membrane at a density of 180,000 cells/cm<sup>2</sup> and incubated for 4 hours. Then the transwell were placed in a 24-multiwell plate and cultured for 48 hours.

Static culture and dynamic culture conditions were investigated. The static condition was achieved by simply keeping the 24-multiwell plate at 37°C, whereas the dynamic condition was implemented with the aid of a microfluidic chip connected with tubes to a perfusion pump. In Figure 16 is schematically explain the two different culture methods.

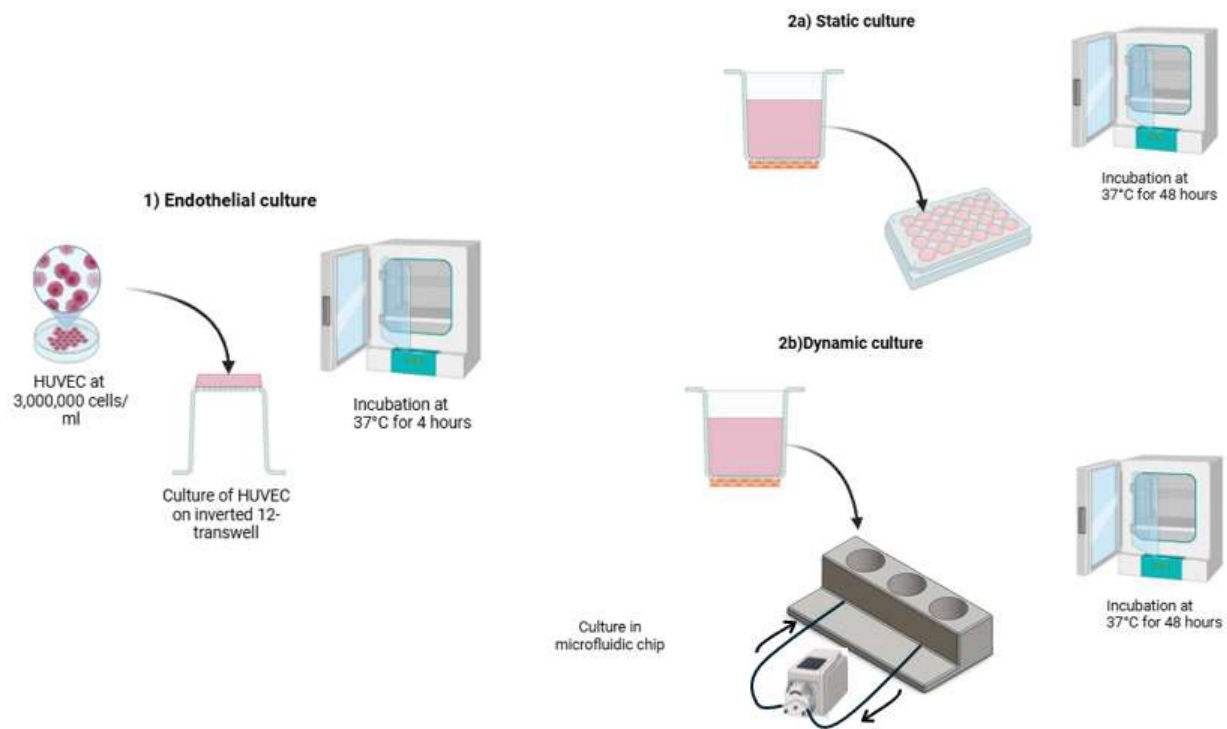


Figure 16: Method for endothelial layer characterization on the bottom side of a transwell membrane. Two conditions were investigated, the static and the dynamic. The static condition was explored by placing the transwell in a 24-multiwell, whereas the dynamic condition was explored by using the microfluidic chip. Illustration created with BioRender.com

### 3.4.2 Endothelial layer maturation

To determine the maturation of the endothelial layer, immunofluorescence analysis for the endothelial markers CD31, ZO1, VE cadherin (VE-CAD) was performed. Briefly. HUVECs were fixed in 4% PFA, permeabilized in 0.5% Triton X-100, and blocked for 45 minutes with Thermo Scientific™ SuperBlock™ Blocking Buffer. Samples were incubated overnight with anti-CD31 monoclonal rabbit antibody (Sigma, SAB5500059, 1:50 dilution), anti-ZO1 monoclonal rabbit mAb antibody (Cell Signalling Technology, D6L1E, 1:200 dilution) and Anti-VE Cadherin antibody Intercellular Junction Marker (Abcam, ab33168, Rabbit, 1:1000). Subsequently, secondary antibody (Goat Anti-Rabbit IgG H&L Alexa Fluor® 555 - Abcam, AB150078, Goat, 1:200 dilution) was incubated

for 1 hour. Negative controls were included in the procedure. HUVEC cells were classified as positive or negative based on the marker expression, with positive staining appearing in red.

### 3.4.3 Vascularized dermal model

To induce dermal model vascularization, endothelial cells were seeded on the basal compartment of a transwell insert as previously described. The dermal model was developed as previously described and, once mature, laced in the apical compartment of the transwell. The model was then cultured under dynamic conditions for up to 10 days in a medium mix of DMEM with 15% FBS and Endothelial culture medium 5 % of ECGS exploiting the microfluidic device as previously described.

The system was incubated at 37°C, and samples were fixed at four different time points: 8 days and 10 days (Figure 17).

Immunostaining for VE-CAD was performed to assess capillary formation within the gel.

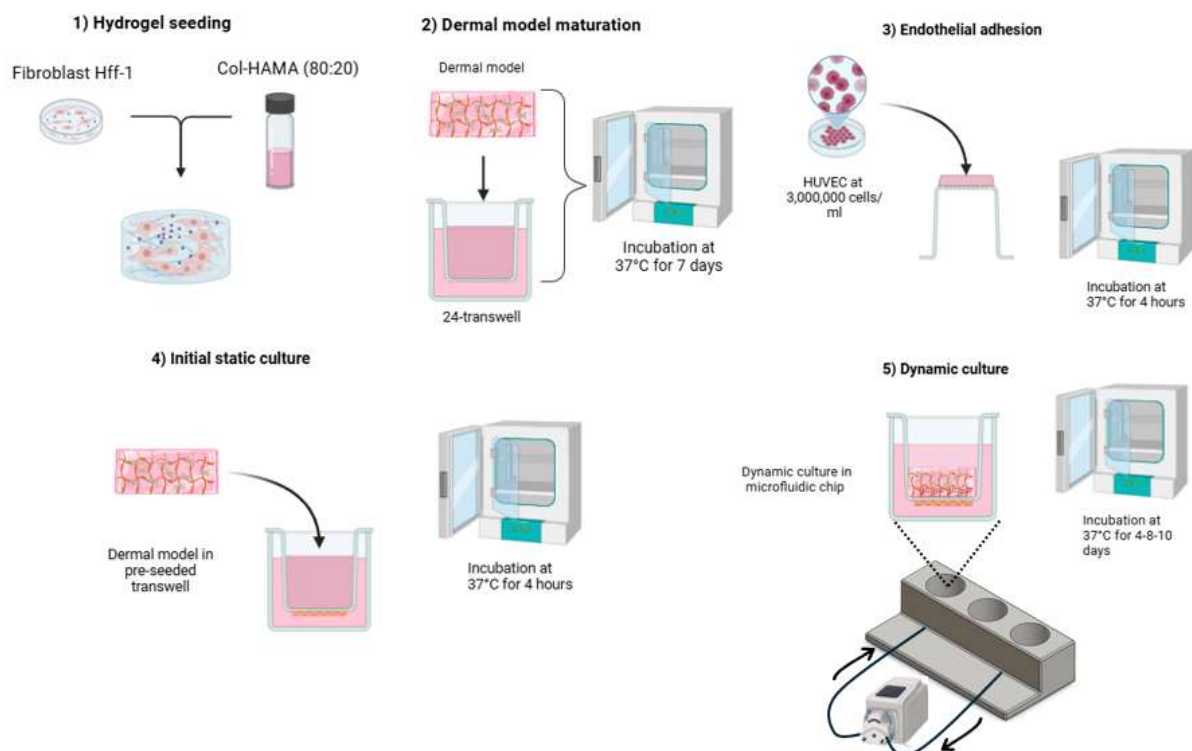


Figure 17: Protocol for generating a vascularized dermal model. After the seeding of the Col-HAMA formulation with fibroblast and after its 7 days maturation, endothelial cells were seeded on the bottom side membrane of the transwell, with 4-hour static incubation to permit cell adhesion. After that the system was placed inside the microfluidic chip and incubated for different time points. Illustration created with BioRender.com

To confirm the integrity of the vascular network obtained in the dermal matrix, fluorescent nanoparticles (NPs) were administered to the vascularized dermal model.

The model was developed as previously described. Fluorescent NPs were administered into the basal compartment of the transwell. Three samples were prepared for each condition and the presence of NPs into the dermal matrix was observed after 1 hour, 3 hours, and 6 hours of incubation through confocal microscopy. (Figure 18)

To localize the capillary network within the dermal matrix, immunofluorescent staining of VE-CAD was performed. Non vascularized dermal model were used as a control.

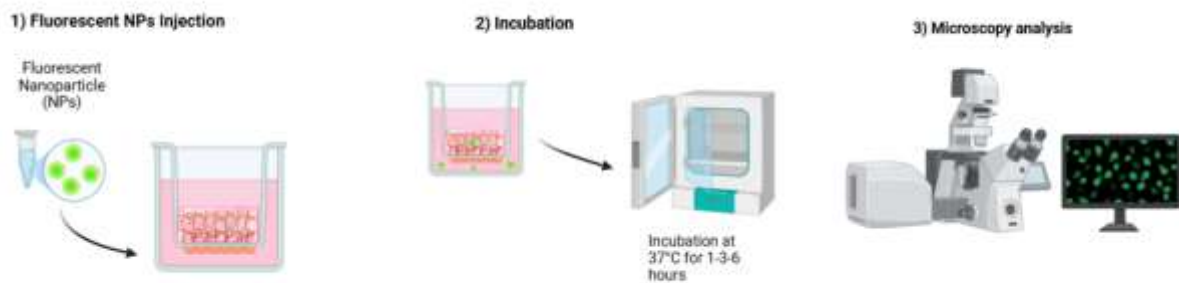


Figure 18: Schematic representation for the administration procedure of NPs. Illustration created with BioRender.com

### 3.5 Statistical analysis

Results are reported as mean  $\pm$  standard deviation. To perform statistical analysis, GraphPad Prism and Microsoft Excel software were used. Imaging analysis was performed thanks to the use of ImageJ software.

# 4 Results

## 4.1 Dermal Model

### 4.1.1 Rheological Test

To begin the rheological test, a time sweep test was performed as the first step in characterizing the materials. During this test, the variation of the storage modulus ( $G'$ ) over time was monitored. The measurement was conducted during the respective photoreticulation and thermoreticulation processes, which allowed for the observation of the changes in the material's mechanical properties.

(Figure 19)

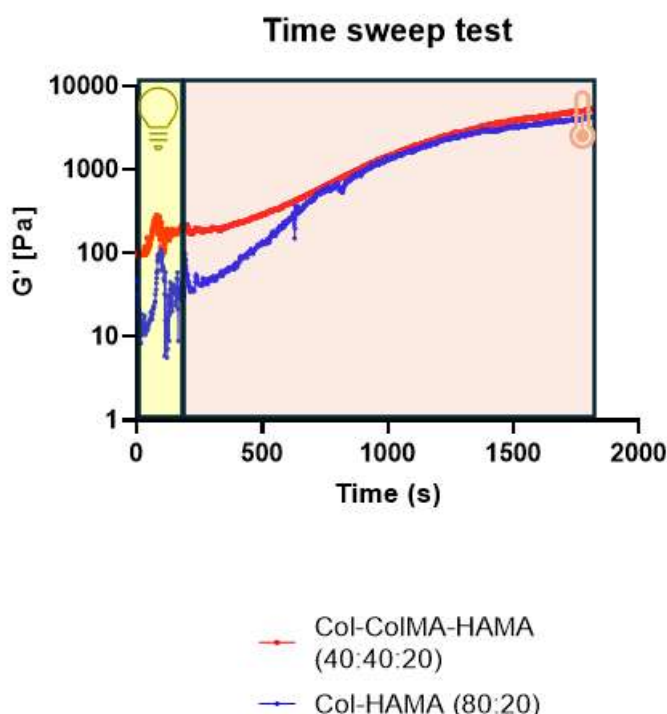


Figure 19: Hydrogel's storage modulus behaviour during frequency sweep test. After an initial phase of photo reticulation of 60 seconds the three formulations undergo a 30-minute phase of thermoreticulation.

During the initial photoreticulation phase, the effect of the exposure to visible light of the formulations can be observed. The  $G'$  modulus begins to increase as the methacrylated groups undergo activation and subsequent crosslinking. Following this phase,  $G'$  stabilizes as thermoreticulation begins. The graph illustrates a continuous increase in  $G'$  until it reaches a plateau, at which point the test was concluded.

In general, the Col-ColIMA-HAMA and Col-HAMA formulations exhibit good mechanical behaviour, as indicated by their final  $G'$  values of 5.3 kPa and 4.5 kPa, respectively.

As expected, the Col-ColIMA-HAMA formulation demonstrates a higher  $G'$  than Col-HAMA due to the presence of additional methacrylate groups on collagen, which enhance hydrogel stiffness during photoreticulation.

Following the crosslinking tests, it was evaluated the behaviour of the gels under varying strain levels through the Strain Sweep test. Figure 20 depict the  $G'$  and  $G''$  of the two formulations.

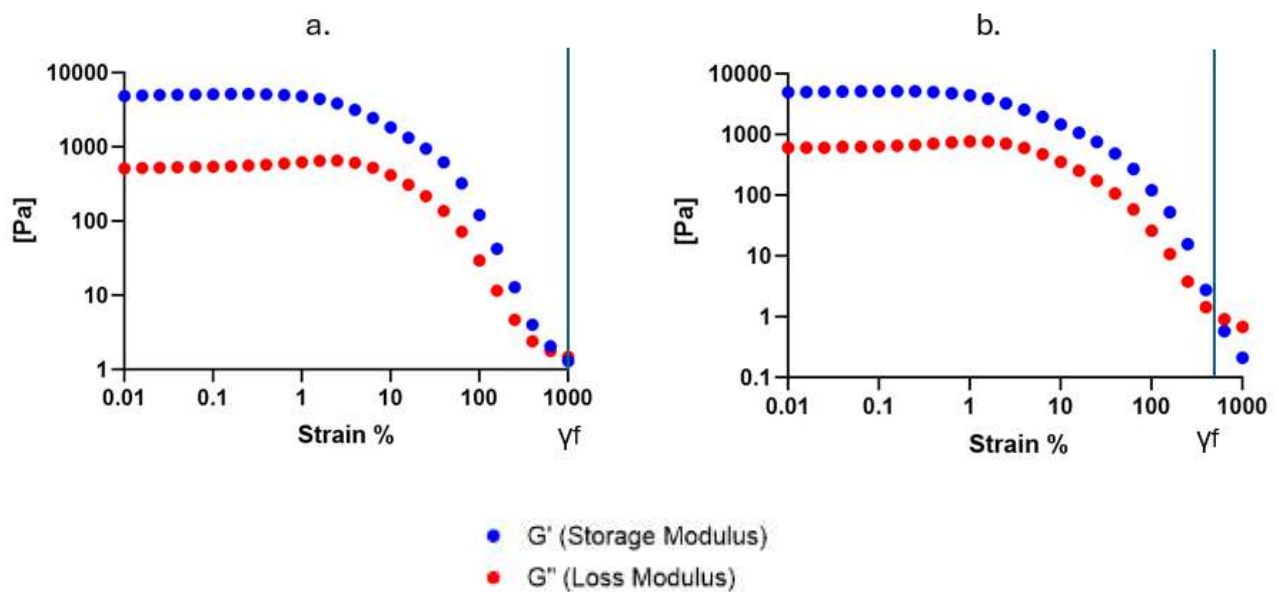


Figure 20: Graphic of the Strain sweep tests conducted on a) Col-HAMA (80:20) and b) Col-ColIMA-HAMA (40:40:20). The tests were performed over a strain range from 0.01% to 1000%. For both formulation the LVE region end at 1% of strain. The  $\gamma_f$  begins at around 1000% and 700% respectively for Col-HAMA and Col-ColIMA-HAMA.

From figure 20, a consistent trend is observed across all formulations. The LVE region, which represents the strain range where the gels maintain their elastic behaviour, extends up to approximately 1% strain for the Col-ColIMA-HAMA and Col-HAMA formulations. Beyond this point, the materials begin to deform non-linearly.

Additionally, the  $\gamma_f$ , which indicates the strain level at which the gels transition into a flow-like state, occurs at 1000% strain for Col-HAMA and at 700% of strain for Col-ColIMA-HAMA.

This test confirms the previous findings from the time sweep test. Specifically, the Col-ColIMA-HAMA and Col-HAMA formulations maintain a  $G'$  modulus of approximately 5000 Pa within the LVE region, aligning with the expected mechanical characteristics of a valid dermal model.

At the end of the linear viscoelastic (LVE) region, all formulations exhibit a gradual decline in  $G'$ . This behaviour suggests that the samples do not undergo brittle fracture but instead demonstrate greater resistance to structural deformations.

Considering the rheological properties of human dermis and the results of these tests, both Col-ColMA-HAMA and Col-HAMA hydrogels appear to meet the necessary mechanical criteria. For this reason, further analysis is required to determine the most suitable material for the intended application.

#### **4.1.2 Cell Viability**

To evaluate the biocompatibility of the considered formulation (ColMA-Col-HAMA (40:40:20), Col-HAMA (80:20)), viability tests were performed via CellTiter blue assay. In Figure 21 are reported the outcomes of the cell viability quantification. Cell viability is expressed as the ratio of the measured value at a given time point to the value recorded on day 1. The results for the Col-ColMA-HAMA formulation reveal a significant decline in cell viability starting from day 7, suggesting that this formulation does not result suitable to sustain fibroblast survival and function within the dermal model. Viability decrease can be attributed to the high stiffness of the matrix which creates an environment that is not conducive to proper fibroblast attachment and proliferation.

Whereas the Col-HAMA formulation demonstrates promising cell viability over time, making it a strong candidate for the dermal model. The data indicate a continuous increase in cell viability from the beginning of the experiment, with an impressive 100% increase in absorbance recorded after 14 days compared to day 1, suggesting that the formulation effectively supports fibroblast attachment, proliferation, and metabolic activity within the hydrogel matrix.

Despite the minor decline in viability over time, the Col-HAMA (80:20) formulation remains the most promising among the tested hydrogels, offering the most favourable biological conditions. Its optimal balance between mechanical stability and cellular compatibility supports fibroblast attachment, proliferation, and survival. Given these properties, this formulation emerges as the best candidate for developing a robust and biologically relevant dermal model.

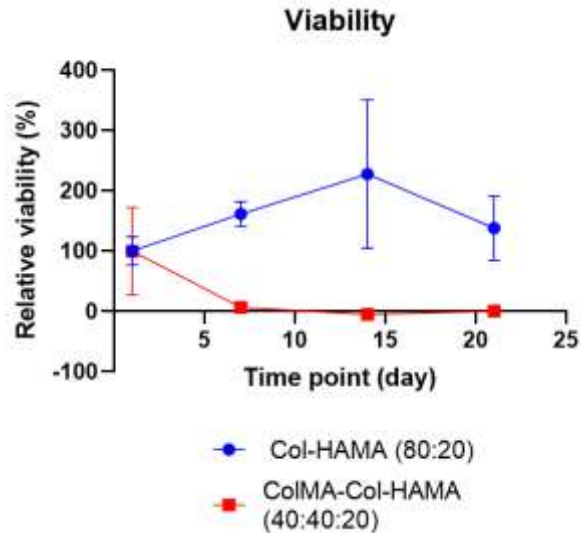


Figure 21: Graphic representation of relative cell viability obtained through CellTiter Blue assay. The Col-ColMA-HA samples presents the worst viability results whereas the Col-HAMA formulation present good biocompatibility properties.

### 4.1.3 Gel Degradation

The Col-HAMA formulation has been identified as the most suitable material for the development of the dermal model. A key factor in its effectiveness is its behaviour under degradative conditions, as maintaining structural integrity over time is essential. The hydrogel must not degrade too rapidly, ensuring that it provides sufficient support until fibroblasts have synthesized and deposited their own extracellular matrix.

Figure 22 illustrates the degradation profile of the hydrogel over time. In figure 22a the wet weight variation of the hydrogel is presented: the formulation initially undergoes a swelling phase during the first few hours after crosslinking. This results in a rapid increase in weight due to water absorption, caused by the bond between water and the free polymeric hydrophilic chain.[51] Once the hydrogel reaches its maximum swelling capacity, it enters a phase of slow and steady degradation, indicating a gradual breakdown of its polymeric network. Notably, after seven days, the hydrogel retains a relative weight comparable to its initial state at 0 hours, demonstrating its structural stability.

Figure 22b illustrates the dry weight variation of the hydrogel. The graph demonstrates an immediate decrease in dry weight, particularly at the initial time points. This rapid reduction can be partially attributed to the hydrolytic degradation of the gel. During this process, vulnerable polymeric chains interact with water molecules, leading to their cleavage into smaller fragments. These fragmented

chains subsequently disperse into the surrounding medium, contributing to the observed weight loss.[52]

These findings highlight the Col-HAMA (80:20) hydrogel's excellent durability and prolonged structural integrity, making it an ideal candidate for cellular support in the dermal model. Its ability to maintain its form while undergoing gradual degradation provides an optimal environment for fibroblast proliferation and extracellular matrix formation, further reinforcing its suitability for the creation of the dermal model.

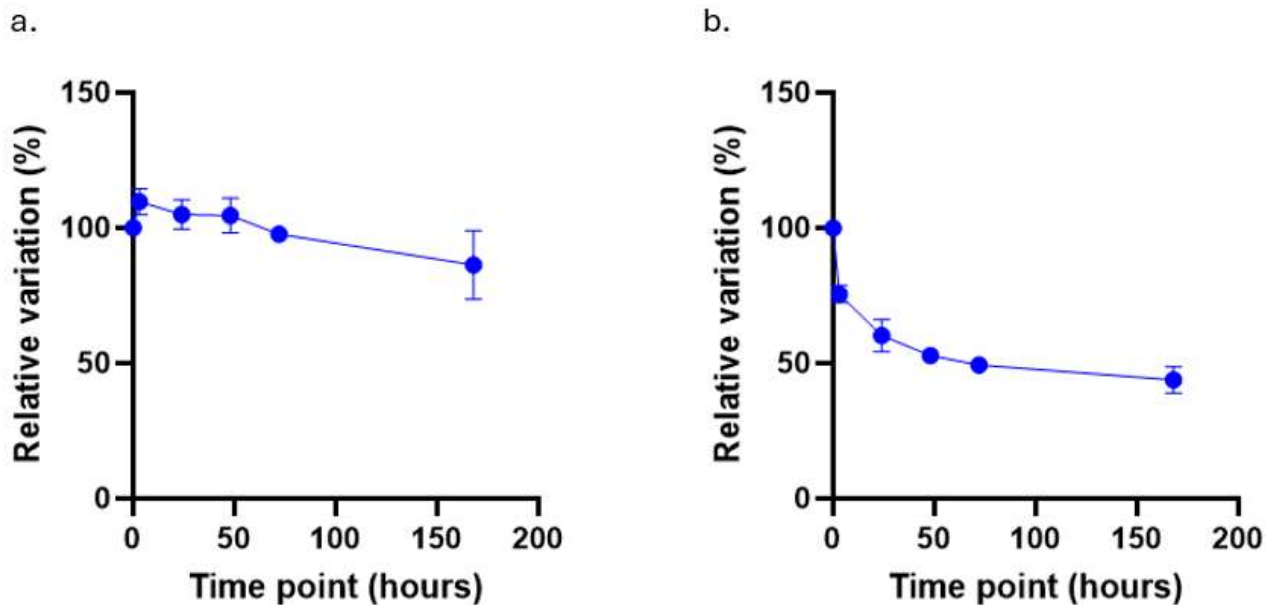


Figure 22: a) Wet weight variation % of Col-HAMA (80:20) formulation. The graphic shows an initial increase of the gel weight, this is mainly due to the swelling process that the gel undergoes in the initial hours. The y-axis represents the weight variation percentage, ranging from 50% to 150%. b) Dry weight variation % of Col-HAMA (80:20) formulation. The gel initially undergoes a rapid decrease in dry weight, likely due to hydrolytic degradation that begins immediately upon exposure to the surrounding environment. After this initial phase, the gel stabilizes and eventually reaches a plateau, indicating a slower degradation rate or equilibrium in the process. The y-axis represents the weight variation percentage, ranging from 0% to 100%.

#### 4.1.4 Native ECM protein deposition

Following the selection and characterization of the Col-HAMA (80:20) hydrogel, a functional dermal model was successfully developed. The initial investigation aimed to evaluate the ability of fibroblasts to degrade the hydrogel and replace it with their own extracellular matrix (ECM). This process is critical, as fibroblasts play a key role in ECM homeostasis *in vivo*. To assess ECM deposition,

immunofluorescence analysis was performed, focusing on the expression of human collagen type I and fibronectin, the primary components of fibroblast-derived ECM.[53]

Figure 23 presents confocal microscopy images of the dermal matrix at various time points. A control sample without cells was included as a reference standard, exhibiting no detectable expression of human collagen type I or fibronectin. This observation confirms the absence of fluorescence signals from the bovine collagen used in hydrogel fabrication.

From the obtained results, it is possible to observe that after seven days of culture, fibroblasts initiate the remodelling of the matrix. At this early stage, a small amount of human collagen type I and fibronectin deposition is observable. By day 14, the presence of native ECM components became significantly more pronounced, indicating that dermal fibroblasts result able to depose native ECM protein when cultured within the model.

By day 21, fibroblasts exhibited signs of structural organization. This structural reorganization is a crucial step in the maturation and functionality of the engineered dermal model.

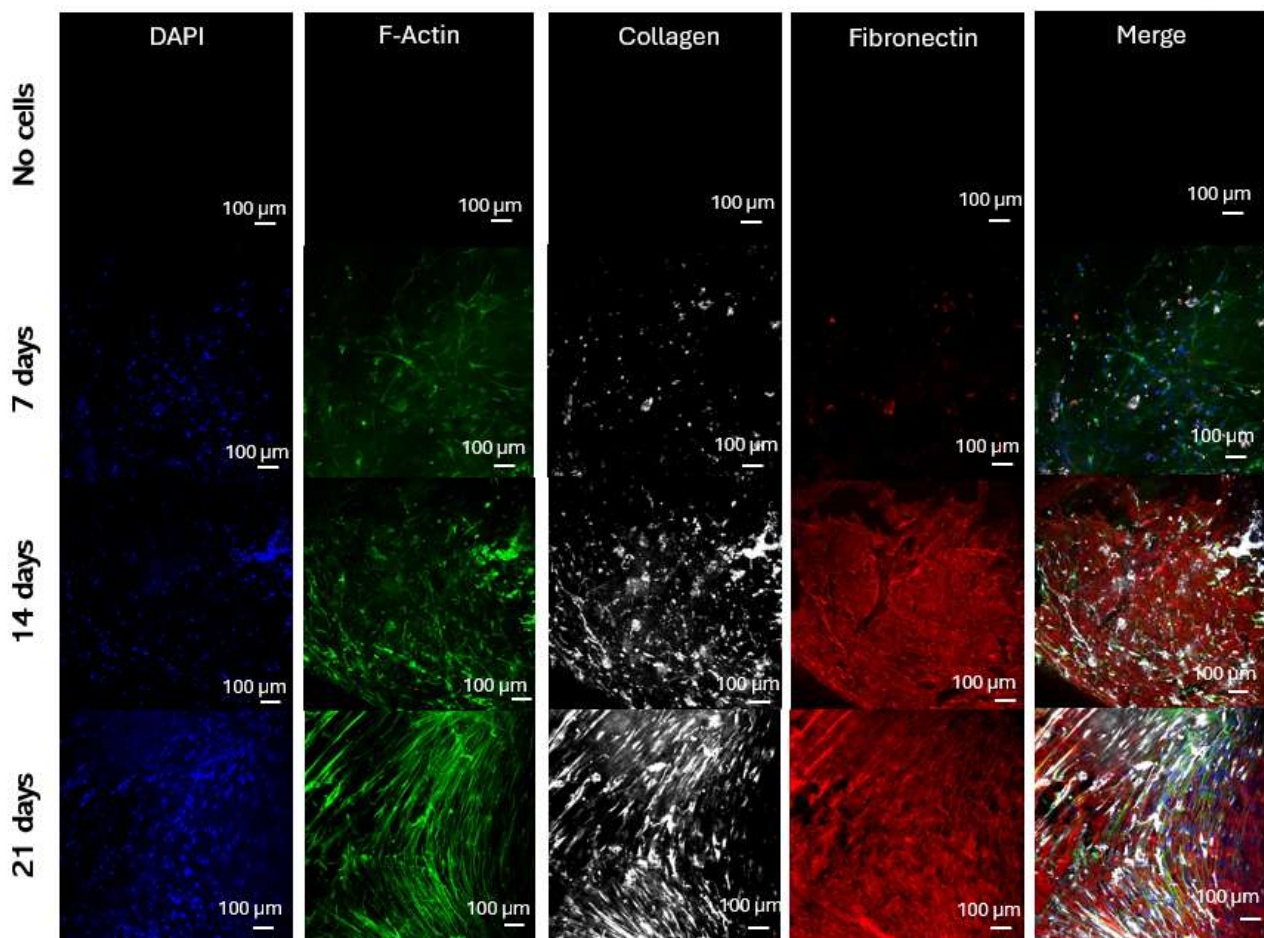


*Figure 23: Immunofluorescence analysis of human collagen and fibronectin deposition. The control does not exhibit any human collagen presence. Whereas, starting for the day 7, fibroblast deposit their own matrix as collagen and fibronectin are markedly expressed.*

## 4.2 Epidermal Model

After successfully reproducing a reliable dermal model, the next step involved generating a stable and mature epidermal layer on top. To achieve this, keratinocytes were seeded onto the dermal model and cultured for four days before being exposed to the air-liquid interface for an additional seven and ten days to complete the maturation process. The objective was to develop a thick keratinocyte layer, clearly distinguishable from the underlying dermal model.

Figure 24 presents an immunofluorescent top-view image of the hydrogel, illustrating the keratinocyte layer covering the dermal structure. The HaCaT cells successfully reached maturation, forming a uniform, continuous layer without gaps between the cells.

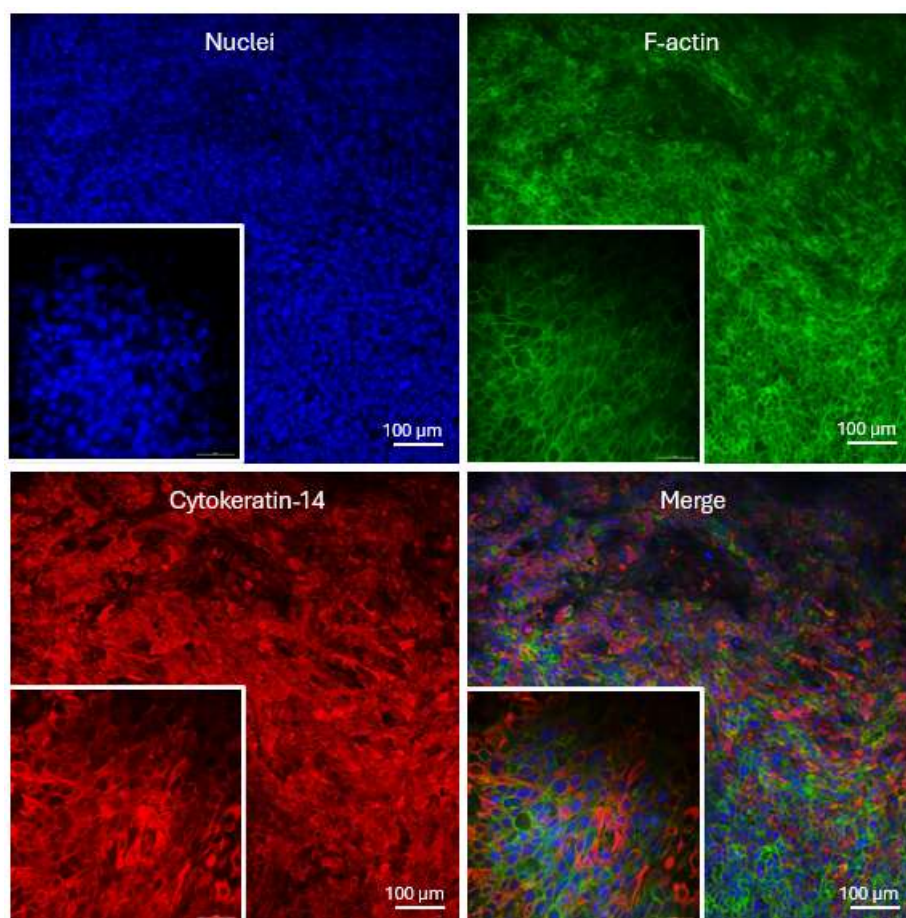


*Figure 24: Immunofluorescence analysis of the epidermal layer. Top view. Keratinocytes have proliferated until the creation of a uniform layer.*

Figure 25 presents a cross-section of the epidermal model, the top section is occupied by the thick epidermal layer composed of stratified keratinocytes, while the bottom section shows the dermal model in which reside fibroblasts. Notably, the keratinocytes seeded during the maturation process at the air-liquid interface have developed a stratified structure. This is evident in the image, where distinct overlapping cell layers can be observed from the surface to the basal region.

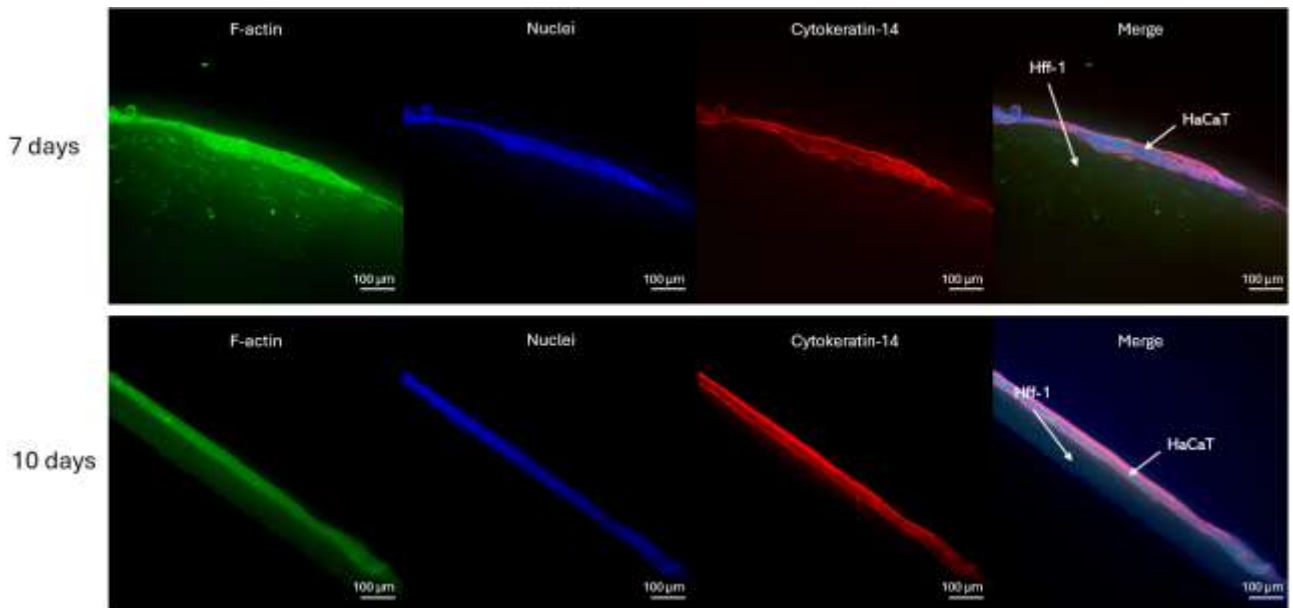


Figure 25: Immunofluorescent illustration of the epidermal layer model on top of the dermal model.

## 4.3 Melanoma Model

The next phase in establishing the primary melanoma model involves the integration of a tumour component into the previously developed dermal model. To achieve this, melanocyte spheroids were introduced into the fibroblast-seeded Col-HAMA hydrogel, and their behaviour was monitored over time.

### 4.3.1 Tumour Propagation

Initially, spheroid expansion was assessed through optical microscopy. Figure 26 illustrates the expansion of SK-MEL spheroids within the hydrogel. Figure 26a shows an SK-MEL spheroid embedded in the Hff-1-seeded hydrogel, while Figure 26b presents an SK-MEL spheroid within the hydrogel in the absence of Hff-1 fibroblasts. In both conditions, no significant morphological changes were observed during the first two time points.

Starting from day 4, the SK-MEL spheroids initiated their invasion and proliferation within the hydrogel, with visible expansion of the spheroid mass. This process continued over the following days, leading to a progressive dispersion of melanoma cells into the surrounding matrix. At this stage, notable differences between the two conditions became evident.

In the absence of fibroblasts (SK-MEL-only condition, figure 26b), melanoma cells exhibited a higher degree of invasion and dispersion throughout the hydrogel. This behaviour may be attributed to the lack of supportive fibroblasts, which play a critical role in remodelling the ECM and establishing a

TME conducive to controlled cell growth. Consequently, by day 10, the SK-MEL spheroids in this condition showed pronounced expansion and a more diffuse cell distribution.

On the contrary, in the SK-MEL + Hff-1 condition (figure 26a), the presence of fibroblasts significantly influenced melanoma cell behaviour. Fibroblasts appeared to impact the invasive capacity of melanoma cells, leading to a more compact tumour spheroid. By day 10, while the spheroid had visibly colonized the surrounding environment, its expansion was more restricted compared to the fibroblast-free condition. This suggests that fibroblasts play a regulatory role in modulating melanoma invasion, potentially by altering the ECM composition and mechanical properties of the hydrogel.[8], [9], [54]

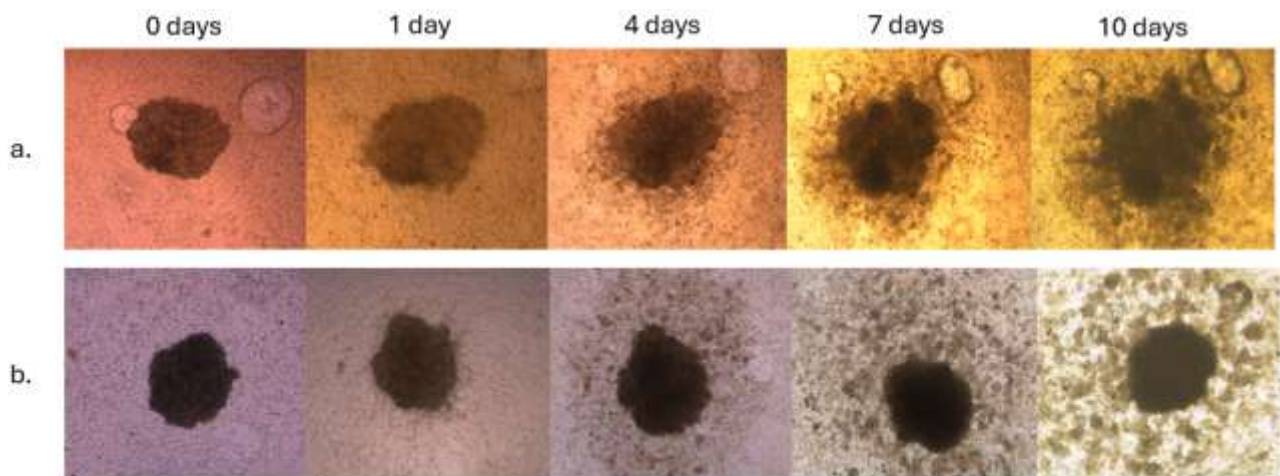


Figure 26: Confront between a) SK-MEL in Hff-1 seeded COL-HAMA hydrogel and b) SK-MEL in COL-HAMA hydrogel. In both condition the SK-MEL spheroid shows an inclination to expand and invade the surrounding environment. The main difference lies in the

#### 4.3.2 Fibroblast and melanocytes interactions

After optical microscopy observation of the melanoma behaviour in the dermal model, the relation between fibroblasts and melanocytes was investigated via immunofluorescence analysis. Firstly, was analysed the expression of MLAN-A protein by melanocytes.

Figure 27a is a 10x magnification images that provides an overall view of the interactions between these two cell types, showing that the elongated fibroblasts tend to support the TME. This interaction is further highlighted in figure 27b (20x), where a direct connection between fibroblasts and melanocytes is evident.

These results confirm the effectiveness of the model in accurately simulating the *in vivo* microenvironment. In physiological conditions, fibroblasts play a crucial role as the primary

supportive component of the TME, and this behaviour is successfully replicated in the model.[8], [10], [54]

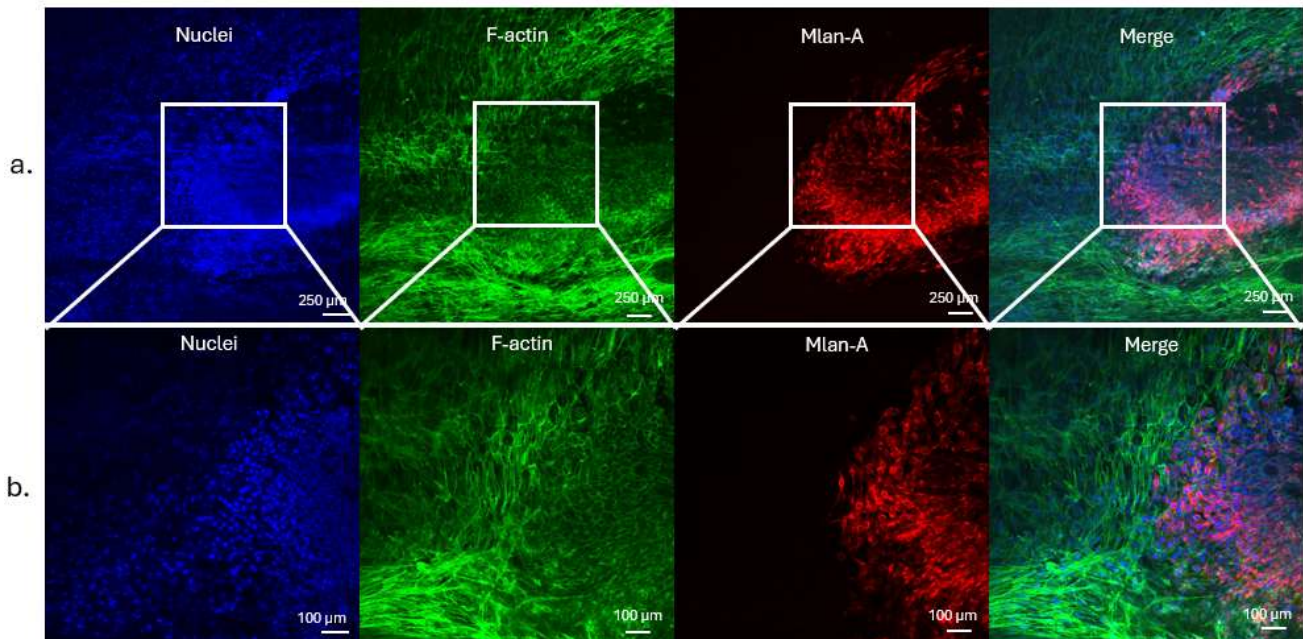


*Figure 27: Fluorescence images of Hff-1 and SK-MEL after a 7-day co-culture at different zoom. a) 10x enlargement. b) 20x enlargement.*

To further analyse the intricate interactions between Hff-1 fibroblasts and SK-MEL melanoma cells, the deposition of Human Collagen I and fibronectin within the tumour spheroid was evaluated following 7 days of culture within the Col-HAMA matrix in single culture (figure 28a) or in co-culture with dermal fibroblasts (figure 28b). To provide a comprehensive analysis of the TME, two different images enlargement of each condition are displayed, enabling both a global and a detailed assessment.

In Figure 28a, the SK-MEL spheroid is solely supported by the COL-HAMA hydrogel. As a result, no human collagen I or fibronectin staining is detected.

Conversely, Figure 28b illustrates the interaction between SK-MEL spheroids and Hff-1 cells. As expected, the Hff-1 fibroblasts play a crucial role in supporting the TME. The images reveal how melanoma cells expand and proliferate, eventually engulfing the fibroblasts within the spheroid structure. Once incorporated, the Hff-1 cells begin producing collagen and fibronectin, actively contributing to ECM formation. This ECM is essential for melanoma cell support and the overall stability of the TME.[6], [7], [8] Notably, this effect is particularly visible at the periphery of the

spheroids, where melanoma cells initiate their invasive behaviour, spreading into the surrounding environment.

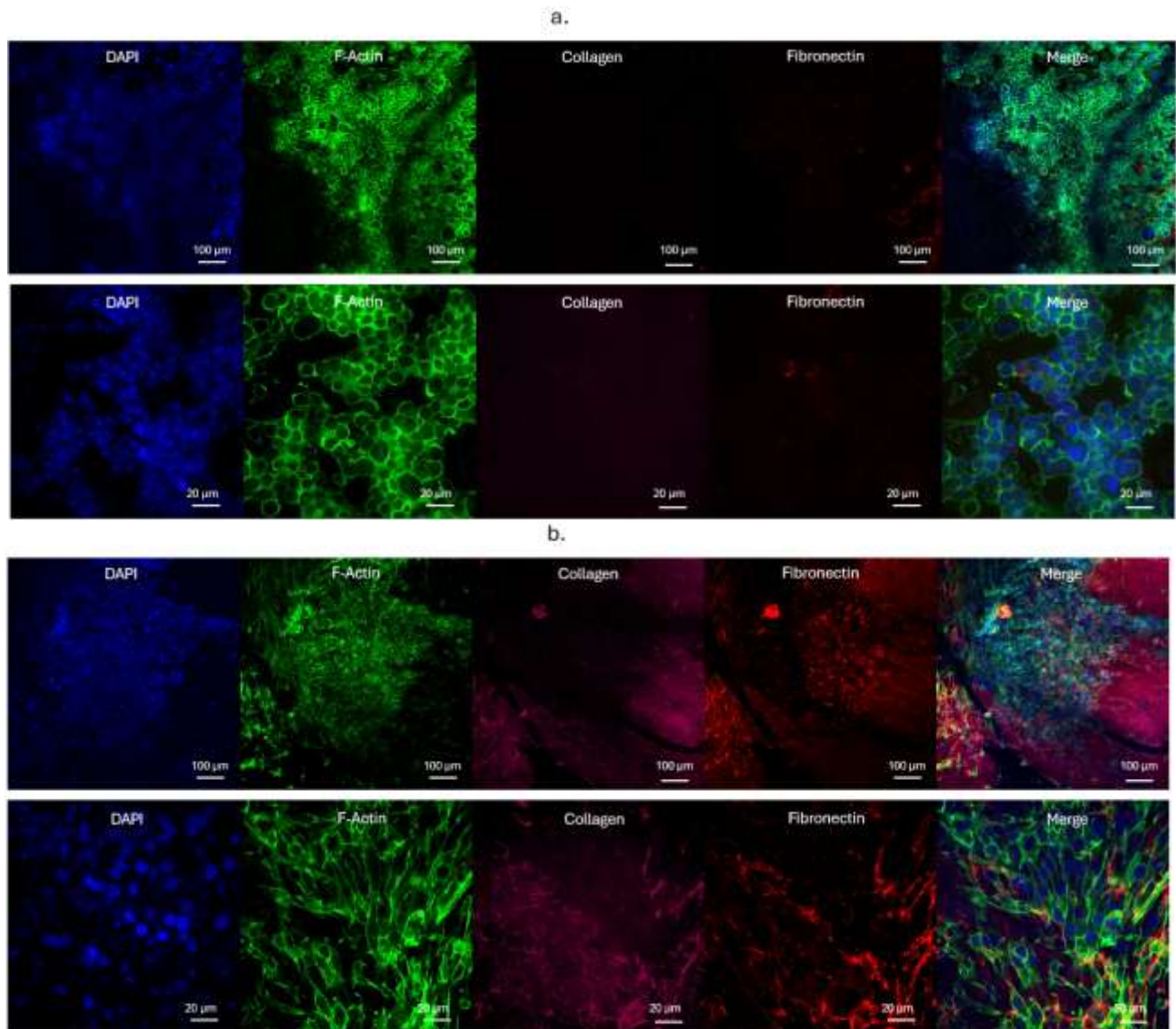


Figure 28: Comparison of collagen and fibronectin expression between SK-MEL only SK-MEL+Hff-1 samples. a) SK-MEL spheroid in Col-HAMA hydrogel at 20x and 60x enlargement. In this case there is no collagen and fibronectin expression as the Hff-1 responsible for their deposition are absent. b) SK-MEL spheroid in Hff-1 seeded COL-HAMA hydrogel at 20x and 60x enlargement. The fibroblast engulfed inside the tumour spheroid have deposited collagen and fibronectin.

### 4.3.3 $\alpha$ -SMA expression

Next, the expression of  $\alpha$ -SMA in fibroblasts was analysed to assess their activation state. When fibroblasts encounter cancer cells, they undergo a transformation into cancer-associated fibroblasts (CAFs).[6], [8], [9], [54] This activation process prompts them to remodel the extracellular matrix and secrete factors that support the inflammatory microenvironment induced by tumour cells. Given the

crucial role of CAFs in tumour progression, the objective of this study was to determine the effect of tumoral melanocytes on fibroblast activation.

To achieve this, different culture conditions were tested, after which immunofluorescence analysis was performed to evaluate  $\alpha$ -SMA expression (Figure 29).

The results were compared with a control sample (figure 29a) to assess variations in fibroblast activation across different conditions. Interestingly, fluorescence analysis revealed significant differences between fibroblasts cultured in conditioned medium (figure 29b) and those subjected to indirect co-culture with tumour cells (figure 29c). Both conditions successfully stimulated fibroblasts to undergo activation and produce  $\alpha$ -SMA, but the indirect co-cultured represents the best solution.

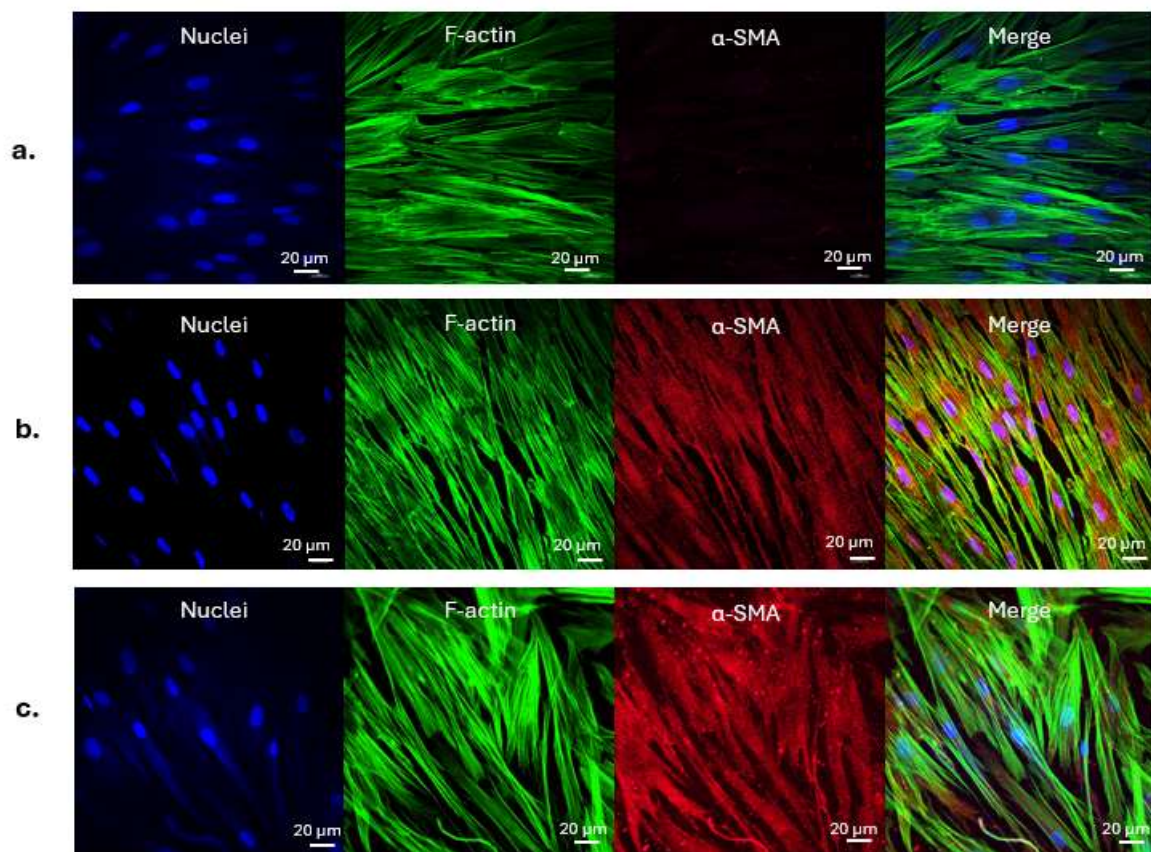


*Figure 29: immunofluorescence analysis of CAF cells in different conditions. a) The control does not show any fluorescence to  $\alpha$ -SMA. b) Conditioned medium culture. The fibroblasts were cultured with melanocytes conditioned medium. The filaments of  $\alpha$ -SMA are visibly expressed. c) Indirect co-culture. The fibroblasts were cultured in multiwell and felt the influence of melanocytes seeded on a transwell place inside the well of the multiwell. This influence is effective as in comparison the control the samples expressed  $\alpha$ -SMA.*

To further quantify fibroblast activation, the percentage of fluorescence positivity was evaluated. This analysis aimed to numerically determine which culture condition was most effective in promoting the production of activated fibroblasts. Figure 30 illustrates the percentage of fluorescence positivity observed in fibroblasts under different experimental conditions.

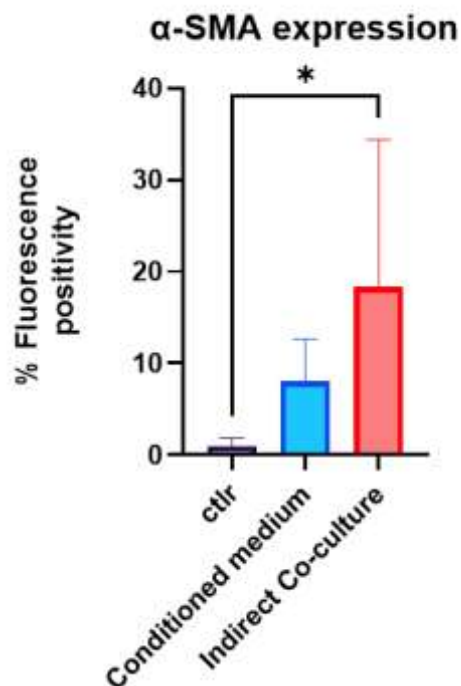


*Figure 30: Analytic comparison of percentage of fluorescence positivity to  $\alpha$ -SMA of the different conditions (number of total images  $n=35$ ). The control shows no expression of  $\alpha$ -SMA as expected, whereas the conditioned medium culture has a good expression, but the better condition for the development of fibroblast expressing  $\alpha$ -SMA is the indirect co-culture.*

The highest level of  $\alpha$ -SMA expression was detected in the indirect co-culture, indicating that this method is the most effective in driving fibroblast activation. As expected, the control samples exhibited the lowest levels of fluorescence positivity, confirming the absence of significant fibroblast activation in the absence of tumour-derived factors.

Interestingly, fibroblasts cultured in conditioned medium displayed intermediate levels of  $\alpha$ -SMA expression. This suggests that while conditioned medium can induce fibroblast activation, its effectiveness is lower than that of direct tumour cell interaction in the indirect co-culture.

In conclusion, the optimal condition for inducing the transformation of fibroblasts into CAF cells is the indirect co-culture of fibroblasts with melanocytes.

## 4.4 Vascularized model

### 4.4.1 Endothelial Cells characterization

As the tumour model was successfully developed and fully functional, the next step involved characterizing the endothelial layer seeded on the bottom side of the transwell membrane, which serves as the foundational base for the vascularized model.

One of the primary distinguishing characteristics of healthy endothelial cells is their shape. Numerous studies have demonstrated that under shear stress, endothelial cells tend to adopt an elongated, elliptical morphology.[55], [56] For this reason, investigating the effect of dynamic conditions on the cells was of interest. Therefore, the cells were cultured under two different conditions: a static condition and a dynamic condition. Immunofluorescence analysis was then employed to assess cell morphology and directionality. Figure 31 presents a comparison between endothelial cells subjected to dynamic and static conditions. The results clearly indicate that shear stress in the dynamic condition (figure 31b) significantly influences the morphology of the endothelial cells, causing them to elongate and align in the shear stress direction. In contrast, endothelial cells cultured in the static condition (figure 31a) exhibit no clear directionality and display a more isotropic shape.

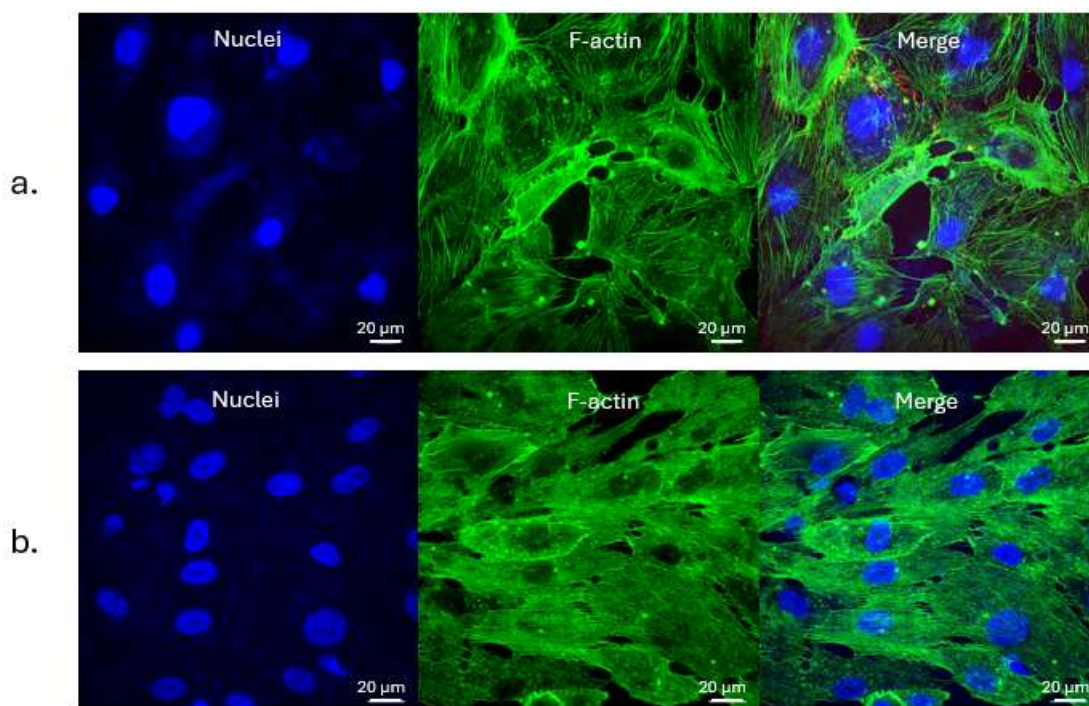


*Figure 31: Immunofluorescence comparison between dynamic and static culture of endothelial cells. a) Static culture. The endothelial cells proliferate in an anisotropic shape not showing any orientation and directionality. b) Dynamic culture. The endothelial cells subjected to dynamic flow tend to take a specific directionality and orientation following the flow lines. They also show an elliptic shape.*

To support the visual directionality observed in the immunofluorescent images, a statistical analysis was conducted. Figure 32 presents the directionality histograms that examines the orientation of endothelial cells under both dynamic (Figure 32a) and static (Figure 32b) conditions.

In both cases, the resulting distribution follows a Gaussian curve, characterized by a peak and a spread of values. The peak indicates the predominant direction adopted by the cells, whereas the amplitude of the curve represents the dispersion of directionality values.

In Figure 32a is observable a single preferential direction, demonstrating a clear directional preference with minimal dispersion. In contrast, Figure 32b reveals a broader distribution, indicating that endothelial cells in the static culture condition exhibit a more random orientation, as evidenced by the high dispersion in the Gaussian curve. This means that the endothelial cell subjected to a dynamic flow tend to adapt and assume its direction, better mimicking the *in vivo* situation.

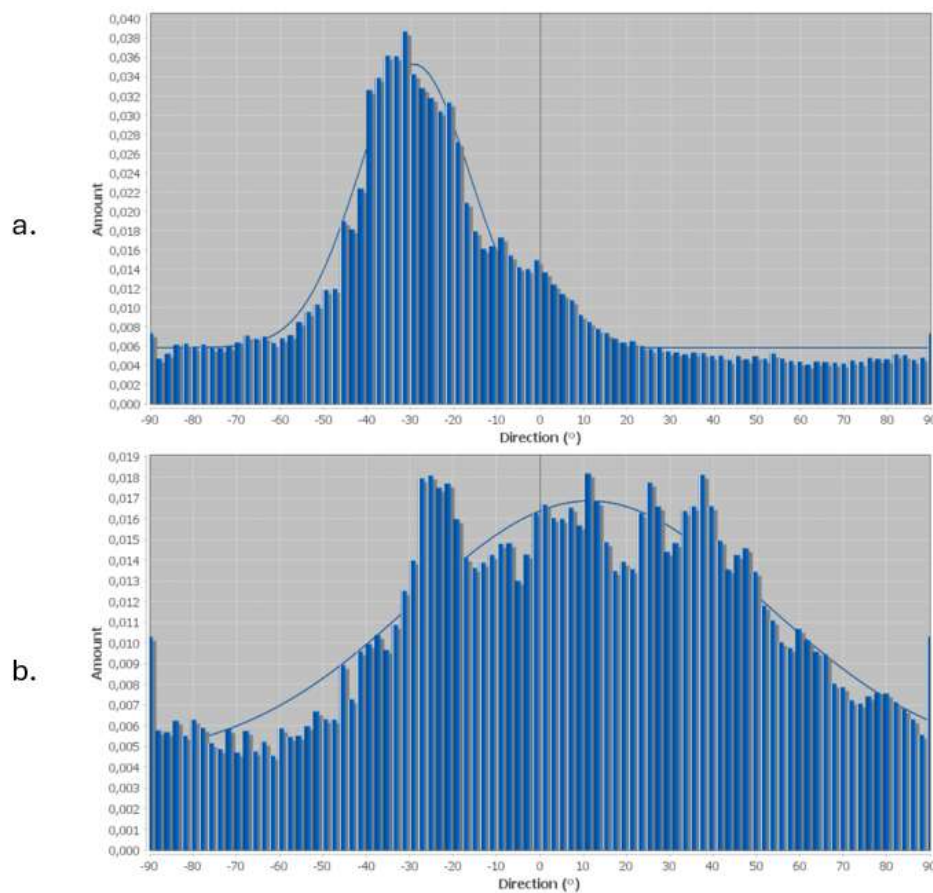


Figure 32: Histogram representation of cell directionality for endothelial cells cultured in a) dynamic condition and b) static condition. Imaging analysis operated with ImageJ on a total of images  $n=33$ .

Beyond evaluating cell shape and alignment, the roundness of endothelial cells was also analysed to further characterize the effects of shear stress on cellular morphology. This additional investigation provides deeper insights into the structural adaptations of endothelial cells cytoskeleton under

different microenvironmental conditions, reinforcing the critical role of mechanical forces in vascular modelling.

Figure 33 presents the roundness measurements derived from the obtained images. The data clearly indicate that endothelial cells cultured under dynamic conditions exhibit significantly lower roundness compared to those maintained in static conditions. In this context, roundness is quantified on a scale where a value of 0 corresponds to a completely elongated or flattened shape, whereas a value of 1 represents a perfectly circular form. These findings further support the notion that shear stress promotes a more elongated endothelial morphology in dynamic conditions, highlighting its crucial role in mimicking physiological vascular environments.

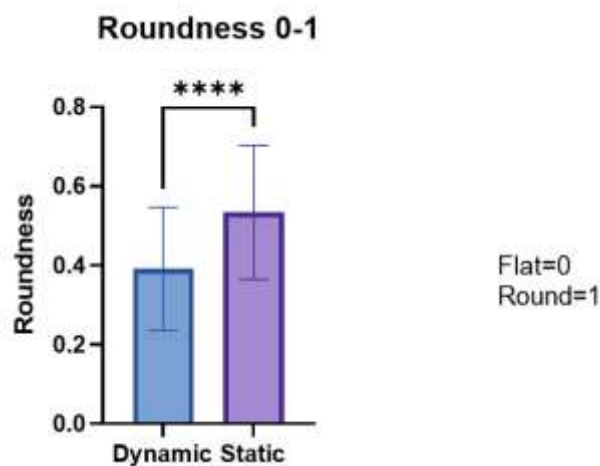


Figure 33: The bar graph represents the roundness of endothelial cells, where 0 corresponds to completely flat cells and 1 to fully round cells. Cells cultured under static conditions exhibit significantly higher roundness compared to those in dynamic conditions suggesting that dynamic culture promotes a more elongated cell morphology. Error bars indicate standard deviation. Number of total ROI investigated  $n=316$ .

Another important feature to consider is the protein expression. Typically, endothelial cells in a healthy environment begin to express specific markers such as ZO-1, VE-Cadherin (VE-CAD), and CD31. These proteins are crucial for cellular adhesion, as they are expressed at the junctions between adjacent cells, facilitating strong intercellular connections. *In vivo*, endothelial cells naturally adhere to one another to maintain the integrity of the vascular system. Therefore, replicating this state *in vitro* is essential for developing a functional endothelial layer. The presence of these markers indicates that the cells are beginning to form a continuous and uniform monolayer, resembling physiological conditions. To validate this assumption, the expression of these markers was investigated under both

static and dynamic conditions. Figure 34 presents fluorescence images obtained through confocal microscopy, comparing the two conditions. The results clearly demonstrate the presence of ZO-1, VE-CAD, and CD31 in endothelial cells cultured under dynamic conditions (figure 34b), whereas these markers are absent in cells maintained under static conditions (figure 34a). This finding further confirms that dynamic conditions provide a healthier and more physiologically relevant environment for endothelial cells, supporting proper cell adhesion and monolayer formation.

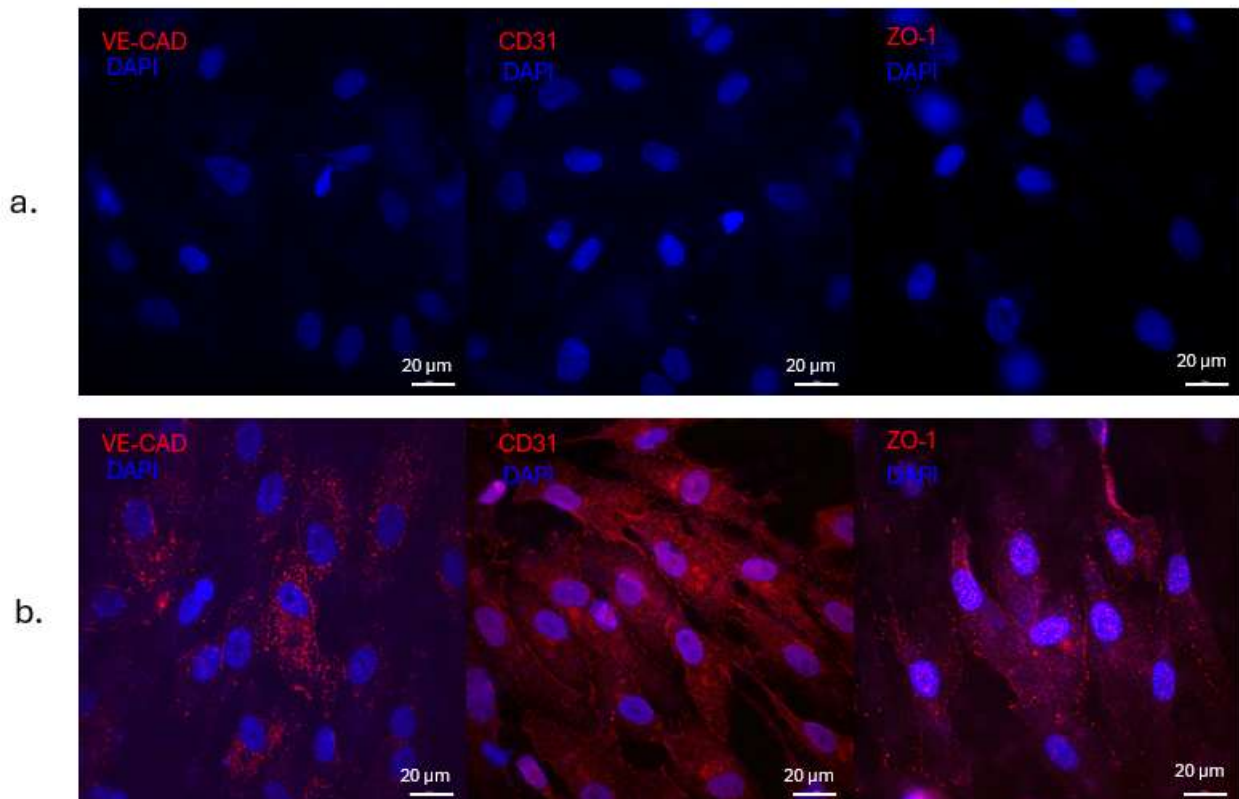


Figure 34: Immunofluorescence analysis of endothelial markers. (a) Cells cultured under dynamic conditions simulating the *in vivo* environment. (b) Cells cultured under static conditions. Endothelial markers are shown in red, while cell nuclei are stained with DAPI.

#### 4.4.2 Vascularized Dermal model

After establishing the dynamic condition as the most suitable environment for endothelial cell culture, the next step was to develop a vascularized dermal model. The goal was to investigate the ability of endothelial cells to assemble into micro vessels within the hydrogel.

The experimental approach involved seeding endothelial cells on the bottom side of the membrane layer, allowing them to migrate across the membrane and into the hydrogel. Once inside, the cells were expected to proliferate and organize into vase-like structures, mimicking the capillary network observed *in vivo*.

Figure 35 illustrates the Col-HAMA (80:20) hydrogel seeded with fibroblasts for 14 days, followed by placement in an HUVEC-seeded transwell and subsequent observation after 8 and 10 days of culture. It can be observed the presence of HUVEC cells inside the Col-HAMA hydrogel. These results provide clear evidence of endothelial cell migration from the transwell membrane into the hydrogel, as demonstrated by the strong expression of the VE-Cadherin marker.

Within the hydrogel, the endothelial cells initiate a self-organizing process. This behaviour leads to the formation of vessel-like structures, which are distinctly visible at both time points. Such self-assembly process suggests an intrinsic ability of the HUVEC to establish a network that mimics the capillary architecture found *in vivo*.

On a macroscopic scale (Figure 35a), the cells tend to organize into a structured reticulum, creating an interconnected network that resembles the early stages of microvascular formation. A closer examination (Figure 35b) further reveals the branching and ramification of these vase-like structures, indicating progressive network maturation over time.

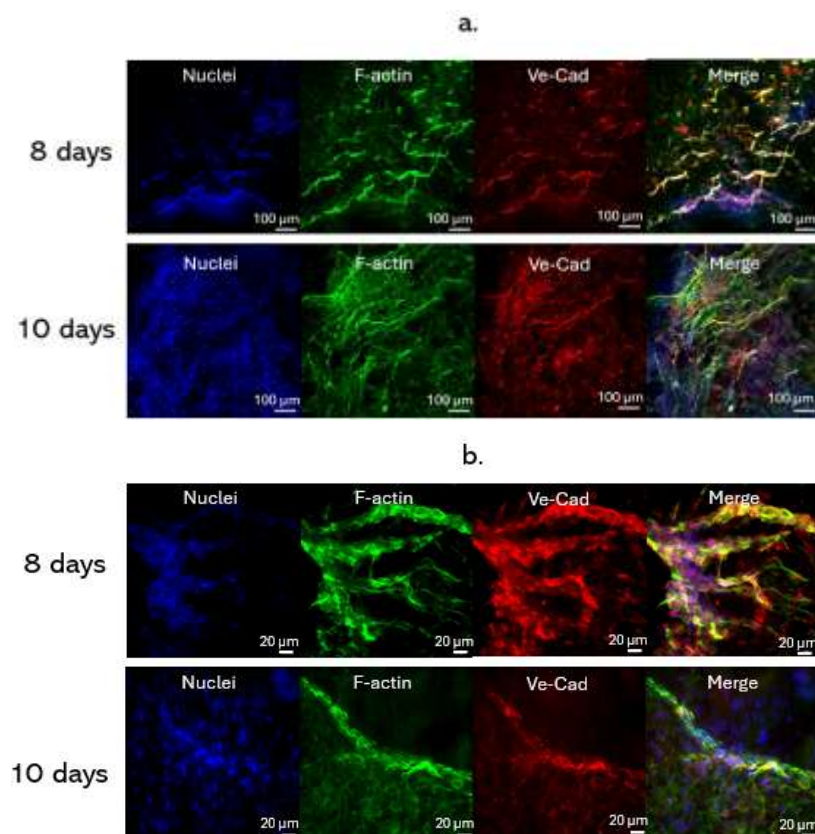
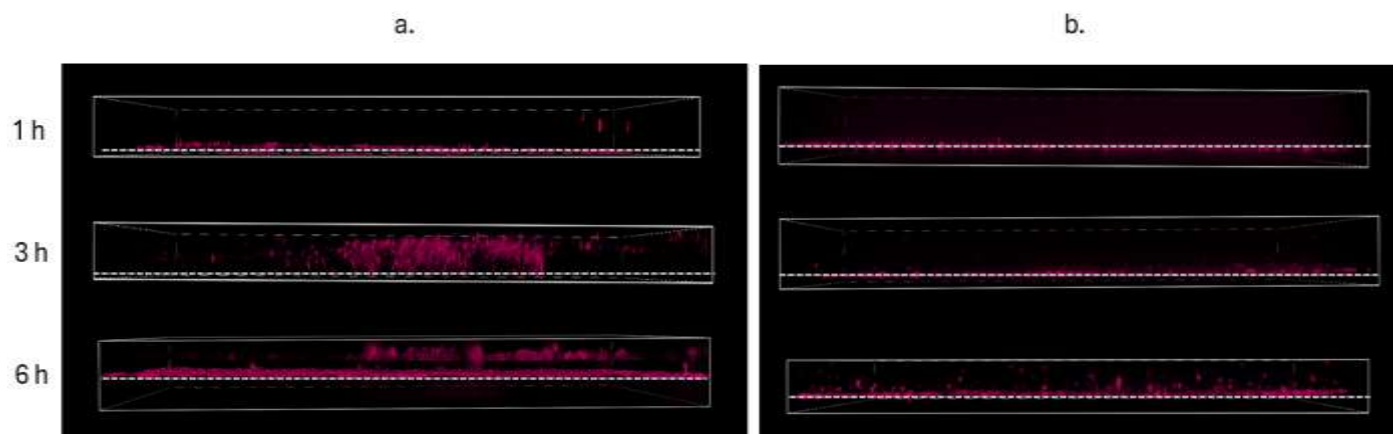


Figure 35: Immunofluorescent images of HUVEC and Hff-1. a) 20 x shot of the sample. It gives a global indication of the behaviour of HUVEC with Hff-1. At 8 days co-culture the endothelial cells supported by the fibroblast begin a self-organization process in vaselike structures. This process is implemented in the 10 days co-culture. b) 60 x shot of the sample. Zoomed view of the vaselike structures where the ramification structure could be observed.

### 4.4.3 Vascular network patency

To confirm the presence of pervious vascular network within the hydrogel, fluorescent NPs were administered to the samples on the basal compartment of the transwell. The NPs were incubated with the model for up to 6 h and the ability of the NPs to migrate within the hydrogel through the vascular network was observed by confocal microscopy (Figure 36a). As a control condition, fluorescent NPs were administered to dermal model where no vascular network was present (Figure 36b).



*Figure 36: Comparison of NP distribution on samples with vasselike structures and without. a) Sample with the presence of vasselike structures. With the passing of time, the NP diffuse inside the fibroblast hydrogel thanks to the presence of the vase structures formed by the HUVEC. b) Sample without the vasselike structures. In contrast with the other sample the NP do not diffuse easily inside the hydrogel as there are no vase structures. The dotted line represents the transwell membrane.*

After 1h of incubation, NPs in the basal compartment of the transwell had limited interaction time with the endothelial cells, resulting in their initial internalization. However, by the 3-hour time point, a notable difference emerged. Where vase-like structures were present, NPs began to diffuse into the hydrogel more effectively, leading to a well-distributed fluorescent signal. In contrast, in the samples where no vascular network was developed, NPs remained confined within the endothelial cells and did not diffuse into the hydrogel. 6 h after the administration of NPs, the previously observed trend is further confirmed: in presence of vascular network within the hydrogel, a uniform fluorescent signal was detected throughout the hydrogel, confirming successful NP diffusion, while the signal in the control samples result nearly absent. This suggests that NPs can still diffuse into the hydrogel, albeit at a slower rate compared to the facilitated diffusion enabled by the vase-like structure.

## 5 Conclusions

This study aimed to develop and characterize a valid model of primary melanoma, with a particular focus on the formation of a vascularized network that closely mimics the capillary system of an *in vivo* melanoma.

To achieve this, a COL-HAMA (80:20) hydrogel was employed as a scaffold, seeded with Hff-1 cells to establish a dermal model. This served as the foundational layer for the melanoma model, within which a melanoma spheroid was embedded. Once the melanoma model was established, a layer of keratinocytes was added to the top of the hydrogel to replicate the epidermal layer.

To further enhance the physiological relevance of the model, a vascularized system was developed using a 24-well transwell insert. The basal side of the transwell membrane was pre-seeded with HUVEC cells to create an endothelial layer. The melanoma model was then placed within the transwell, allowing for the observation of HUVEC cell infiltration and organization within the hydrogel. The primary objective was to facilitate the formation of a structured vascular network resembling the capillary system.

The results obtained highlight the successful reproduction of a viable and reliable dermal model. This was confirmed through immunofluorescence analysis, which demonstrated the presence of human collagen and fibronectin within the samples. These findings indicate that the Hff-1 cells seeded in the COL-HAMA hydrogel actively degraded the scaffold and deposited their own ECM, thereby enhancing the biomimicry of the model.

Following the establishment of a robust dermal layer, the next step was the development of a physiologically relevant epidermal model. To achieve this, HaCaT cells were seeded on top of the dermal construct and, after a four-day culture period, exposed to an air-liquid interface. This approach facilitated the formation of a well-structured epidermal layer, as confirmed by immunofluorescence analysis, which revealed a thick layer of epithelial cells covering the dermal model.

Subsequently, the melanoma model was developed by embedding a melanoma spheroid within the dermal construct. The interactions between Hff-1 and SK-MEL were closely examined, with a particular focus on their dynamic relationship. The results indicated that fibroblasts responded to the presence of melanoma cells by actively remodelling the TME and producing ECM components to support melanoma progression. Immunofluorescence analysis further validated this observation by highlighting the significant presence of human collagen and fibronectin within the TME, reinforcing the supportive role of fibroblasts in melanoma development.

Additionally, optical microscopy provided further confirmation of these findings. A comparative analysis between fibroblast-supported spheroids and melanoma spheroids cultured without fibroblasts revealed notable structural differences. Specifically, spheroids supported by Hff-1 fibroblasts exhibited a more compact and cohesive morphology, suggesting an enhanced ECM-mediated stabilization of the tumour structure.

Following the successful establishment of the melanoma model, the final step was the induction of vascularization within the tumour construct. To achieve this, the process began with the characterization of the basal endothelial layer on the underside of a 24-transwell membrane, which served as the starting point for endothelial cell migration and the formation of vessel-like structures within the hydrogel.

It was determined that the most effective method for achieving a uniform endothelial layer was dynamic culture within a microfluidic chip. Once this optimized culture condition was established, the fibroblast-seeded COL-HAMA hydrogel was placed inside the transwell, allowing for the observation of endothelial cell invasion and proliferation within the gel matrix.

Immunofluorescence analysis confirmed the successful formation of vascular-like structures. Initially, this was evidenced by the presence of organized endothelial markers within the hydrogel, resembling *in vivo* blood vessels. Additionally, the use of fluorescent NPs provided further validation, as their diffusion over time within the hydrogel demonstrated functional permeability and network connectivity, reinforcing the physiological relevance of the model.

The findings of this study have significant implications for the development of a reliable melanoma model with potential applications in drug testing. However, certain limitations still need to be addressed. One major challenge is the use of natural polymers, such as collagen, which, despite their excellent biological properties, exhibit inherent batch-to-batch variability. Additionally, the immunofluorescent visualization of multiple cell types within the same sample remains challenging due to the limited availability of species-specific immunomarkers. As a result, only two distinct markers can be observed simultaneously within a single sample.

To overcome these challenges, further optimization of the system is required to enable the seamless integration of all components. Enhancing the reproducibility and multiplexed imaging capabilities of the model will be crucial for improving its applicability in preclinical research.

Looking ahead, the use of a three-chamber microfluidic chip represents a promising avenue for advancing this model. Such a system would allow for the observation, development, and systemic release of tumour metastases in a controlled environment. Specifically, the melanoma model could

be placed in the first chamber, while the other two chambers could house healthy tissues, such as brain or lung tissue, common metastatic targets of melanoma. This setup would provide a more comprehensive understanding of metastatic behaviour and facilitate the development of targeted therapeutic strategies against metastatic cancer.

This thesis has contributed to a deeper understanding of the development of a metastatic melanoma model. Despite its limitations, the proposed approach represents a significant step forward in the field of drug development, with the potential to evolve into a state-of-the-art system for drug testing. Furthermore, this study advances research on metastatic melanoma by providing a robust foundation for future investigations. By addressing current challenges and optimizing the model, future work can further enhance its applicability, ultimately improving preclinical testing and therapeutic strategies for metastatic melanoma.

## 6 Ringraziamenti

La conclusione di questo percorso di studi rappresenta per me un traguardo importante, raggiunto grazie al supporto di molte persone a cui desidero esprimere la mia più sincera gratitudine.

Comincerei con il ringraziare la Prof.ssa Mattu e Carlotta che mi hanno seguito e aiutato durante lo svolgimento e la stesura della mia ricerca di tesi magistrale, dimostrando pazienza e tatto anche in questi ultimi momenti difficili del mio percorso, e che hanno contribuito alla mia personale crescita accademica e professionale.

La mia eterna gratitudine va alla mia famiglia, Mamma, Papà, Marta, Matteo, Angela e Nonna sempre presenti, davanti a qualsiasi cosa, a supporto con una mano sulla spalla, senza mai frenarmi, piuttosto guidandomi nel mio percorso di crescita. Grazie per i valori che avete instillato nella mia persona, spingendomi sempre con l'obiettivo di far emergere la versione migliore di me nonostante le difficoltà che spesso il percorso di vita ci pone davanti.

Un grazie particolare ai membri dell'On-Off Staff, Serra, Galfio e Migno, miei compagni fedeli in questi anni di avventure, con cui il confronto mai banale ha portato alla mia formazione ideologica e sociale. Ricordo ancora il giorno di quella lontana settimana comunitaria in cui ci siamo ritrovati casualmente nella stessa stanza e con estrema naturalezza abbiamo creato questo magnifico legame, ad altre migliaia delle nostre avventure assieme.

A Gio, il mio compare da tanti anni, con cui condivido mille passioni e con cui ho condiviso mille avventure.

Ad Ale, la mia Gym Bro, alcuni dicono la mia versione al femminile. In questi anni di convivenza abbiamo condiviso tanto, e sicuramente continueremo a farlo nonostante la maggiore distanza. Grazie di avermi insegnato di come la vita vada affrontata sempre a testa alta, nonostante tutte le difficoltà.

A Simo, grazie per aver illuminato le nostre giornate accademiche con il tuo sorriso. Nonostante l'attuale distanza un pensiero va sempre a te, costantemente in prima linea per prendersi cura delle persone che ti stanno accanto. Grazie per essermi stata vicino in più di un'occasione e per avermi supportato nelle difficoltà di questo percorso.

Allo Zio Richi, figura di riferimento fin dalla mia infanzia. Una guida da cui prendere esempio e spunto umanamente e intellettualmente. Grazie per avermi mostrato le diverse sfaccettature del nostro quotidiano rispondendo ai miei dubbi e alle mie perplessità senza mai imprimere la tua idea bensì cercando di spingendomi al confronto e al dibattito.

Al gruppo degli Xtreme Merenderos, con cui ho condiviso mille risate, avventure e gioie andando oltre alla passione che ci accumuna.

Un grazie speciale alla Montagna, il mio luogo sicuro e rifugio. Non sei solo neve, dirupi, creste, torrenti, laghi e pascoli, sei un modo di vivere, un passo dopo l'altro, in silenzio, con calma e misura.

*"Io chiedo ad una scalata non solamente le difficoltà ma una bellezza di linee"*

*Walter Bonatti*

## 7 Bibliography

- [1] "Tissue viability," 2017. [Online]. Available: [www.nursing-standard.co.uk](http://www.nursing-standard.co.uk)
- [2] P. A. Kolarsick, M. Ann Kolarsick, and C. Goodwin, "Anatomy and Physiology of the Skin," 2006.
- [3] R. Wong, S. Geyer, W. Weninger, J. C. Guimberteau, and J. K. Wong, "The dynamic anatomy and patterning of skin," *Exp Dermatol*, vol. 25, no. 2, pp. 92–98, Feb. 2016, doi: 10.1111/exd.12832.
- [4] W. D. Losquadro, "Anatomy of the Skin and the Pathogenesis of Nonmelanoma Skin Cancer," Aug. 01, 2017, *W.B. Saunders*. doi: 10.1016/j.fsc.2017.03.001.
- [5] H. H. Bragulla and D. G. Homberger, "Structure and functions of keratin proteins in simple, stratified, keratinized and cornified epithelia," in *Journal of Anatomy*, 2009, pp. 516–559. doi: 10.1111/j.1469-7580.2009.01066.x.
- [6] R. Rimal *et al.*, "Cancer-associated fibroblasts: Origin, function, imaging, and therapeutic targeting," Oct. 01, 2022, *Elsevier B.V.* doi: 10.1016/j.addr.2022.114504.
- [7] J. Mazurkiewicz *et al.*, "Melanoma cells with diverse invasive potential differentially induce the activation of normal human fibroblasts," *Cell Communication and Signaling*, vol. 20, no. 1, Dec. 2022, doi: 10.1186/s12964-022-00871-x.
- [8] R. A. Glabman, P. L. Choyke, and N. Sato, "Cancer-Associated Fibroblasts: Tumorigenicity and Targeting for Cancer Therapy," Aug. 01, 2022, *MDPI*. doi: 10.3390/cancers14163906.
- [9] R. Melchionna, P. Trono, A. Di Carlo, F. Di Modugno, and P. Nisticò, "Transcription factors in fibroblast plasticity and CAF heterogeneity," Dec. 01, 2023, *BioMed Central Ltd*. doi: 10.1186/s13046-023-02934-4.
- [10] J. Wang, R. Zohar, and C. A. McCulloch, "Multiple roles of  $\alpha$ -smooth muscle actin in mechanotransduction," Feb. 01, 2006, *Academic Press Inc*. doi: 10.1016/j.yexcr.2005.11.004.
- [11] J. W. Shin *et al.*, "Molecular mechanisms of dermal aging and antiaging approaches," *Int J Mol Sci*, vol. 20, no. 9, May 2019, doi: 10.3390/ijms20092126.
- [12] G. C. Leonardi *et al.*, "Cutaneous melanoma: From pathogenesis to therapy (Review)," Apr. 01, 2018, *Spandidos Publications*. doi: 10.3892/ijo.2018.4287.
- [13] C. Garbe *et al.*, "European consensus-based interdisciplinary guideline for melanoma. Part 1: Diagnostics: Update 2022," Jul. 01, 2022, *Elsevier Ltd*. doi: 10.1016/j.ejca.2022.03.008.
- [14] A. Slominski, J. Wortsman, A. J. Carlson, L. Y. Matsuoka, C. M. Balch, and M. C. Mihm, "Special Article Malignant Melanoma An Update," 2001.
- [15] O. S. Cherepakhin, Z. B. Argyenyi, and A. S. Moshiri, "Genomic and transcriptomic underpinnings of melanoma genesis, progression, and metastasis," Jan. 01, 2022, *MDPI*. doi: 10.3390/cancers14010123.
- [16] S. Raimondi, M. Suppa, and S. Gandini, "Melanoma epidemiology and sun exposure," *Acta Derm Venereol*, vol. 100, no. 100-year theme Skin malignancies, pp. 250–258, 2020, doi: 10.2340/00015555-3491.
- [17] V. W. Rebecca, R. Somasundaram, and M. Herlyn, "Pre-clinical modeling of cutaneous melanoma," Dec. 01, 2020, *Nature Research*. doi: 10.1038/s41467-020-15546-9.
- [18] B. C. Bastian, "The molecular pathology of melanoma: An integrated taxonomy of melanocytic neoplasia," *Annual Review of Pathology: Mechanisms of Disease*, vol. 9, pp. 239–271, 2014, doi: 10.1146/annurev-pathol-012513-104658.
- [19] J. A. Curtin *et al.*, "Distinct Sets of Genetic Alterations in Melanoma," 2005. [Online]. Available: [www.nejm.org](http://www.nejm.org)
- [20] R. M. Hoffman, "Patient-derived orthotopic xenograft (PDOX) models of melanoma," Sep. 01, 2017, *MDPI AG*. doi: 10.3390/ijms18091875.
- [21] L. K. Smith, A. D. Rao, and G. A. McArthur, "Targeting metabolic reprogramming as a potential therapeutic strategy in melanoma," *Pharmacol Res*, vol. 107, pp. 42–47, May 2016, doi: 10.1016/j.phrs.2016.02.009.
- [22] A. Uong and L. I. Zon, "Melanocytes in development and cancer," Jan. 2010. doi: 10.1002/jcp.21935.

- [23] J. Mazurkiewicz *et al.*, “Melanoma cells with diverse invasive potential differentially induce the activation of normal human fibroblasts,” *Cell Communication and Signaling*, vol. 20, no. 1, Dec. 2022, doi: 10.1186/s12964-022-00871-x.
- [24] R. Rimal *et al.*, “Cancer-associated fibroblasts: Origin, function, imaging, and therapeutic targeting,” Oct. 01, 2022, *Elsevier B.V.* doi: 10.1016/j.addr.2022.114504.
- [25] M. Marzagalli, N. D. Ebelt, and E. R. Manuel, “Seminars in Cancer Biology Review Unraveling the crosstalk between melanoma and immune cells in the tumor microenvironment.”
- [26] C. Garbe *et al.*, “European consensus-based interdisciplinary guideline for melanoma. Part 1: Diagnostics: Update 2022,” Jul. 01, 2022, *Elsevier Ltd.* doi: 10.1016/j.ejca.2022.03.008.
- [27] L. Tagliaferri *et al.*, “Immunotherapy and radiotherapy in melanoma: a multidisciplinary comprehensive review,” 2022, *Taylor and Francis Ltd.* doi: 10.1080/21645515.2021.1903827.
- [28] M. Ralli *et al.*, “Immunotherapy in the Treatment of Metastatic Melanoma: Current Knowledge and Future Directions,” 2020, *Hindawi Limited.* doi: 10.1155/2020/9235638.
- [29] E. A. Grimm, A. ~viazumder, H. Z. Zhang, and S. A. Rosenberg, “LYMPHOKINE-ACTIVATED KILLER CELL PHENOMENON Lysis of Natural Killer-resistant Fresh Solid Tumor Cells by Interleukin 2-activated Autologous Human Peripheral Blood Lymphocytes.”
- [30] V. Niederlova, O. Tsyklauri, M. Kovar, and O. Stepanek, “IL-2-driven CD8+ T cell phenotypes: implications for immunotherapy,” Nov. 01, 2023, *Elsevier Ltd.* doi: 10.1016/j.it.2023.09.003.
- [31] E. Simeone and P. A. Ascierto, “Immunomodulating antibodies in the treatment of metastatic melanoma: The experience with anti-CTLA-4, anti-CD137, and anti-PD1,” *J Immunotoxicol*, vol. 9, no. 3, pp. 241–247, Jul. 2012, doi: 10.3109/1547691X.2012.678021.
- [32] G. Nomdedeu-Sancho *et al.*, “In Vitro Three-Dimensional (3D) Models for Melanoma Immunotherapy,” Dec. 01, 2023, *Multidisciplinary Digital Publishing Institute (MDPI).* doi: 10.3390/cancers15245779.
- [33] K. Duval *et al.*, “Modeling physiological events in 2D vs. 3D cell culture,” Jun. 14, 2017, *American Physiological Society.* doi: 10.1152/physiol.00036.2016.
- [34] A. Marconi, M. Quadri, A. Saltari, and C. Pincelli, “Progress in melanoma modelling in vitro,” May 01, 2018, *Blackwell Publishing Ltd.* doi: 10.1111/exd.13670.
- [35] C. P. Miller *et al.*, “Therapeutic targeting of tumor spheroids in a 3D microphysiological renal cell carcinoma-on-a-chip system,” *Neoplasia (United States)*, vol. 46, Dec. 2023, doi: 10.1016/j.neo.2023.100948.
- [36] T. Ishiguro, H. Ohata, A. Sato, K. Yamawaki, T. Enomoto, and K. Okamoto, “Tumor-derived spheroids: Relevance to cancer stem cells and clinical applications,” Mar. 01, 2017, *Blackwell Publishing Ltd.* doi: 10.1111/cas.13155.
- [37] A. Raza *et al.*, “Oxygen Mapping of Melanoma Spheroids using Small Molecule Platinum Probe and Phosphorescence Lifetime Imaging Microscopy,” *Sci Rep*, vol. 7, no. 1, Dec. 2017, doi: 10.1038/s41598-017-11153-9.
- [38] L. S. Farhoumand *et al.*, “Blockade of  $\beta$ -Adrenergic Receptors by Nebivolol Enables Tumor Control Potential for Uveal Melanoma in 3D Tumor Spheroids and 2D Cultures,” *Int J Mol Sci*, vol. 24, no. 6, Mar. 2023, doi: 10.3390/ijms24065894.
- [39] Z. Zhang and B. B. Michniak-Kohn, “Tissue engineered human skin equivalents,” Mar. 2012. doi: 10.3390/pharmaceutics4010026.
- [40] M. Berning, S. Prätzel-Wunder, J. R. Bickenbach, and P. Boukamp, “Three-Dimensional in Vitro Skin and Skin Cancer Models Based on Human Fibroblast-Derived Matrix,” *Tissue Eng Part C Methods*, vol. 21, no. 9, pp. 958–970, Sep. 2015, doi: 10.1089/ten.tec.2014.0698.
- [41] J. A. Bouwstra, R. W. J. Helder, and A. El Ghalbzouri, “Human skin equivalents: Impaired barrier function in relation to the lipid and protein properties of the stratum corneum,” Aug. 01, 2021, *Elsevier B.V.* doi: 10.1016/j.addr.2021.05.012.
- [42] P. Haridas, J. A. McGovern, S. D. L. McElwain, and M. J. Simpson, “Quantitative comparison of the spreading and invasion of radial growth phase and metastatic melanoma cells in a three-

dimensional human skin equivalent model,” *PeerJ*, vol. 2017, no. 9, 2017, doi: 10.7717/peerj.3754.

- [43] C. Ma, Y. Peng, H. Li, and W. Chen, “Organ-on-a-Chip: A New Paradigm for Drug Development,” Feb. 01, 2021, *Elsevier Ltd*. doi: 10.1016/j.tips.2020.11.009.
- [44] F. Karras and M. Kunz, “Patient-derived melanoma models,” Jul. 01, 2024, *Elsevier GmbH*. doi: 10.1016/j.prp.2024.155231.
- [45] J. M. Ayuso *et al.*, “Microfluidic model with air-walls reveals fibroblasts and keratinocytes modulate melanoma cell phenotype, migration, and metabolism,” *Lab Chip*, vol. 21, no. 6, pp. 1139–1149, Mar. 2021, doi: 10.1039/d0lc00988a.
- [46] P. Herreros, A. López-Hernández, M. Holgado, and M. F. L. Heras, “Melanoma-on-a-chip model for anticancer drug injecting delivery method,” *SLAS Technol*, vol. 29, no. 6, p. 100219, Dec. 2024, doi: 10.1016/j.slast.2024.100219.
- [47] “Wound healing and the role of fibroblasts”.
- [48] H. Kurose, “Cardiac fibrosis and fibroblasts,” Jul. 01, 2021, *MDPI*. doi: 10.3390/cells10071716.
- [49] S. Linder, “Cytokeratin markers come of age,” 2007, *IOS Press BV*. doi: 10.1159/000107582.
- [50] G. Bioley *et al.*, “Melan-A/MART-1-Specific CD4 T Cells in Melanoma Patients: Identification of New Epitopes and Ex Vivo Visualization of Specific T Cells by MHC Class II Tetramers 1,” 2006. [Online]. Available: <http://journals.aai.org/jimmunol/article-pdf/177/10/6769/1227170/zim02206006769.pdf>
- [51] V. M. Gun’ko, I. N. Savina, and S. V. Mikhalovsky, “Properties of water bound in hydrogels,” Dec. 01, 2017, *MDPI AG*. doi: 10.3390/gels3040037.
- [52] A. J. Feliciano, C. van Blitterswijk, L. Moroni, and M. B. Baker, “Realizing tissue integration with supramolecular hydrogels,” Apr. 01, 2021, *Acta Materialia Inc*. doi: 10.1016/j.actbio.2021.01.034.
- [53] J. W. Shin *et al.*, “Molecular mechanisms of dermal aging and antiaging approaches,” *Int J Mol Sci*, vol. 20, no. 9, May 2019, doi: 10.3390/ijms20092126.
- [54] X. Geng *et al.*, “Cancer-Associated Fibroblast (CAF) Heterogeneity and Targeting Therapy of CAFs in Pancreatic Cancer,” Jul. 15, 2021, *Frontiers Media S.A.* doi: 10.3389/fcell.2021.655152.
- [55] “Mechanism of endothelial cell shape change and cytoskeletal remodeling in”.
- [56] D. A. Chistiakov, A. N. Orekhov, and Y. V. Bobryshev, “Effects of shear stress on endothelial cells: go with the flow,” Feb. 01, 2017, *Blackwell Publishing Ltd*. doi: 10.1111/apha.12725.
- [57] N. Kharouf *et al.*, “Tumor Microenvironment as a Therapeutic Target in Melanoma Treatment,” Jun. 01, 2023, *Multidisciplinary Digital Publishing Institute (MDPI)*. doi: 10.3390/cancers15123147.